cmgh
CELLULAR AND MOLECULAR GASTROENTEROLOGY AND HEPATOLOGY

ORIGINAL RESEARCH

COVID-19 Diarrhea is Inflammatory, Caused by Direct Viral Effects Plus Major Role of Virus-induced Cytokines

Mark Donowitz,[1,3] Chung-Ming Tse,[1] Rafiq Sarker,[1] Ruxian Lin,[1] Karol Dokladny,[5] Manmeet Rawat,[5] Ivy Horwitz,[7] ChunYan Ye,[7] George McNamara,[1] Julie In,[5] Alison Kell,[5] Chenxu Guo,[4] Shang JuiTsai,[4] Tyrus Vong,[1] Andrew Karaba,[2] Varsha Singh,[1] Jaiprasath Sachithanandham,[6] Andy Pekosz,[6] Andrea Cox,[2] Steven Bradfute,[5,7] Nicholas C. Zachos,[1] Steven Gould,[4] and Olga Kovbasnjuk[1,5]

[1]Division of Gastroenterology and Hepatology, Department of Medicine, The Johns Hopkins University School of Medicine, Baltimore, Maryland; [2]Division of Infectious Diseases, Department of Medicine, The Johns Hopkins University School of Medicine, Baltimore, Maryland; [3]Department of Physiology, Department of Medicine, The Johns Hopkins University School of Medicine, Baltimore, Maryland; [4]Department of Biological Chemistry, Department of Medicine, The Johns Hopkins University School of Medicine, Baltimore, Maryland; [5]Department of Internal Medicine, University of New Mexico Health Sciences Center, Albuquerque, New Mexico; [6]Department of Microbiology and Immunology, Bloomberg School of Public Health of the Johns Hopkins University, Baltimore, Maryland; and [7]University of New Mexico Center for Global Health, Albuquerque, New Mexico

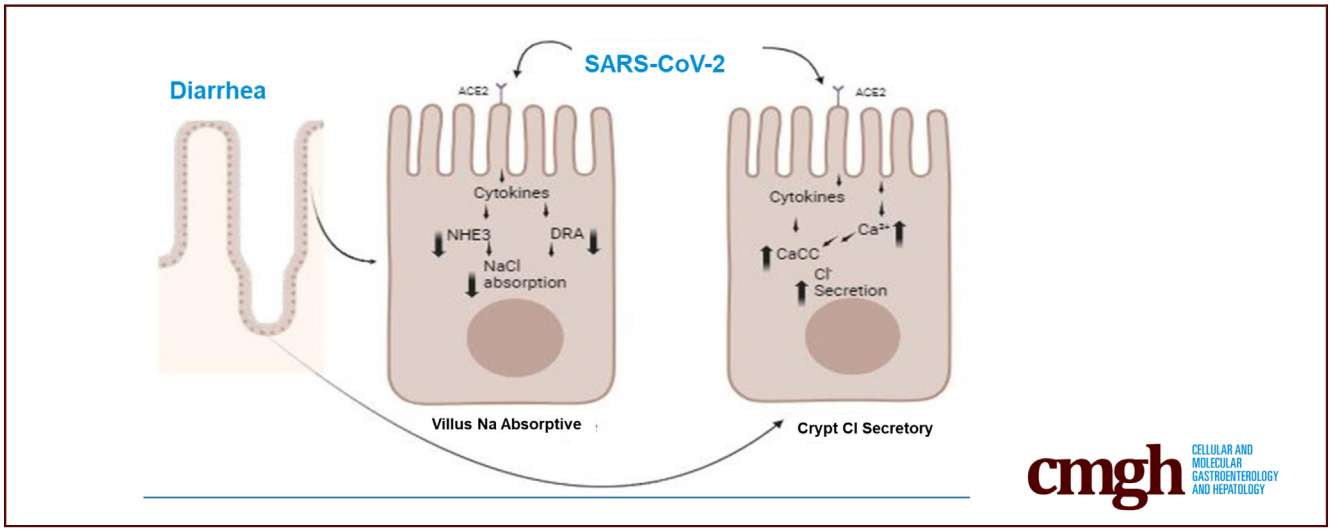

SUMMARY

The pathogenesis of acute COVID-19 diarrhea involves direct viral effects (elevation of intracellular Ca^{2+}, contribution to anion secretion, inflammatory response) and effects of the virus-induced inflammatory response (inhibition of NHE3 and DRA, contribution to anion secretion).

BACKGROUND & AIMS: Diarrhea occurs in up to 50% of cases of COVID-19. Nonetheless, the pathophysiologic mechanism(s) have not been determined.

METHODS: This was examined using normal human enteroid monolayers exposed apically to live SARS-CoV-2 or non-replicating virus-like particles (VLPs) bearing the 4 SARS-CoV-2 structural proteins or irradiated virus, all of which bound and entered enterocytes.

RESULTS: Live virus and VLPs incrieased secretion of multiple cytokines and reduced mRNAs of ACE2, NHE3, and DRA. Interleukin (IL)-6 plus IL-8 alone reduced NHE3 mRNA and protein and DRA mRNA and protein. Neither VLPs nor IL-6 plus IL-8 alone altered Cl^- secretion, but together they caused Cl^- secretion, which was Ca^{2+}-dependent, CFTR-independent, blocked partially by a specific TMEM16A inhibitor, and entirely by a general TMEM16 family inhibitor. VLPs and irradiated virus, but not IL-6 plus IL-8, produced Ca^{2+} waves that began within minutes of VLP exposure, lasted for at least 60 minutes, and were prevented by pretreatment with apyrase, a P2Y1 receptor antagonist, and general TMEM16 family inhibitor but not by the specific TMEM16A inhibitor.

CONCLUSIONS: The pathophysiology of COVID-19 diarrhea appears to be a unique example of a calcium-dependent inflammatory diarrhea that is caused by direct viral effects plus the virus-induced intestinal epithelial cytokine secretion. *(Cell Mol Gastroenterol Hepatol 2024;18:101383; https://doi.org/10.1016/j.jcmgh.2024.101383)*

Keywords: CaCC; Cytokines; Diarrhea; DRA; NHE3; SARS-CoV-2; Virus-like Particles.

COVID-19 causes changes in most organ systems, although the mechanisms appear to vary from direct viral effects to changes due to induction of local or systemic inflammation. The gastrointestinal tract is commonly affected in COVID-19 infection, and diarrhea occurs in up of 50% of acute cases. Diarrhea is also a symptom in up to 30% of long COVID cases and predicts failure for long COVID to resolve within 2 years.[1-15] SARS-CoV-2 infects enterocytes and is detected in intestinal cells of up to 50% of patients dying with COVID-19.[16,17] Some aspects of the pathophysiology of COVID-19 diarrhea have been determined, including that ACE2, the major SARS-CoV-2 receptor, and TMPRSS2, the protease that cleaves the SARS-CoV-2 spike protein and allows viral entry, are highly expressed in the small intestinal enterocyte brush border, where the virus enters enterocytes.[18] Until now, COVID-19 diarrhea has not been characterized in a way the provides mechanistic insights into pathogenesis. For instance, it is not known if the diarrhea is small intestinal or colonic, or secretory or inflammatory. The current study was designed to bridge the following gaps in understanding COVID-19 diarrhea: (1) Given that diarrhea pathophysiology in most cases can be understood as due to reduced Na^+ absorption with or without stimulated Cl^- secretion,[19-21] what are the functional changes in Na^+ and Cl^- transporting proteins in COVID-19 diarrhea? (2) Can changes in transport protein function be attributed to changes in the second messengers that serve as intermediates in most diarrheal diseases? (3) Do known Sars-Cov-2 induced cytokine responses contribute to changes in transport function leading to diarrhea, and how does this occur? Our studies demonstrate that in COVID-19 diarrhea, the same transport processes are altered that contribute to other diarrheal diseases, with inhibition of neutral NaCl absorption and stimulation of anion secretion, with the changes in anion secretion being Ca^{2+} dependent. The elevated intracellular Ca^{2+} occurs in the form of Ca^{2+} waves that start within minutes of SARS-CoV-2 exposure. This diarrheal disease has additional unique aspects. These include that these changes result from a combination of direct viral effects on epithelial cells plus the effects of virus-induced local cytokine secretion, and that the anion secretion is CFTR-independent and rather involves members of the TMEM16 family of calcium-activated Cl^- channels.

Results

Live SARS-CoV-2 Enters and Reproduces in Human Enteroid Monolayers

The apical membranes of differentiated human duodenal and proximal colonic enteroid monolayers were exposed to 10^6 plaque-forming units (PFUs)/ml live SARS-CoV-2 for 90 minutes, washed, and then studied for up to 5 days. Apical and basolateral media were collected 2 and 5 days post-infection, and in addition, enteroids were lysed, and all fractions were studied for viral nucleocapsid mRNA determined by quantitative reverse transcription polymerase chain reaction (qRT-PCR) with concentration of virus particles (VPs/ml) corresponding to mRNA levels calculated from calibration curves. At both 48 and 120 hours after SARS-CoV-2 exposure, VPs were present in apical and basolateral media and from cell lysates from both duodenum and colon, with duodenal levels exceeding colonic levels. This was consistent with greater viral replication in small intestine than colon (Figure 1*A*). Viral entry and replication was confirmed by identifying intracellular double stranded RNA (dsRNA antibody [*red*]) and viral Spike protein (*green*); viral entry occurred in most enterocytes (Spike present), but dsRNA was less uniformly present. Entry did not occur in goblet cells (Figure 1*B*). Insufficient enteroendocrine cells and Tuft cells were identified to allow statement if SARS-CoV-2 enters these cells. Spike protein and dsRNA were not detected in uninfected monolayers studied in parallel as a negative control (Figure 1*C*). In the studies shown in Figure 1*B*, infectious SARS-CoV-2 was detected in colonic enteroid monolayers, as well as in apical media by Vero cell plaque-forming assay but was not consistently detected in the basolateral media (Figure 1*D*). Viral infection did not alter the percent of 10 and 70 kDa fluorescein-dextran that moved from the monolayer apical to basolateral surface in 48 hours (Figure 1*E*). This is consistent with there being no change in intestinal permeability caused by the virus. These results support that SARS-CoV-2 is taken up by enterocytes, reproduces in the enterocytes, and that live virus exits the apical surface.

Live SARS-CoV-2 Infection Causes Cytokine Secretion From Human Enteroids

Because SARS-CoV-2 infection has been reported to affect organs by both direct viral effects and by inducing cytokine release, the effect of apical 10^6 PFUs/ml live SARS-CoV-2 exposure for 90 minutes was determined on duodenal enteroid release of a limited number of cytokines 48 hours after apical exposure (Figure 2). Viral exposure significantly increased duodenal enteroid release of cytokines measured on the basolateral surface. There was significant increase in concentrations of IL-6, monocyte chemoattractant protein-1 (MCP-1), and IL-1β and non-significant increases in IL-8 and tumor necrosis factor (TNF)-α. To mimic the effect of the systemic cytokine elevation on the enteroids, these experiments were repeated in the presence of basolateral (BL) IL-6 plus IL-8 for 48 hours, which led to significant increases in TNF-α and IL-1β secretion both in the presence and absence of virus. The concentration of IL-6 and IL-8 selected was selected to mimic a robust systemic inflammatory response.

Abbreviations used in this paper: **ANOVA, analysis of variance; BL, basolateral; CaCC, calcium-activated Cl^- channel; dsRNA, double-stranded RNA; HEPES, hydroxyethyl piperazine ethanesulfonic acid; IF, immunofluorescence; IL, interleukin; MCP-1, monocyte chemoattractant protein-1; PBS, phosphate buffered saline; PFU, plaque-forming unit; qRT-PCR, quantitative reverse transcription polymerase chain reaction; SEM, standard error of the mean; TNF, tumor necrosis factor; VLP, virus-like particle; VP, virus particle.**

Most current article

2352-345X
https://doi.org/10.1016/j.jcmgh.2024.101383

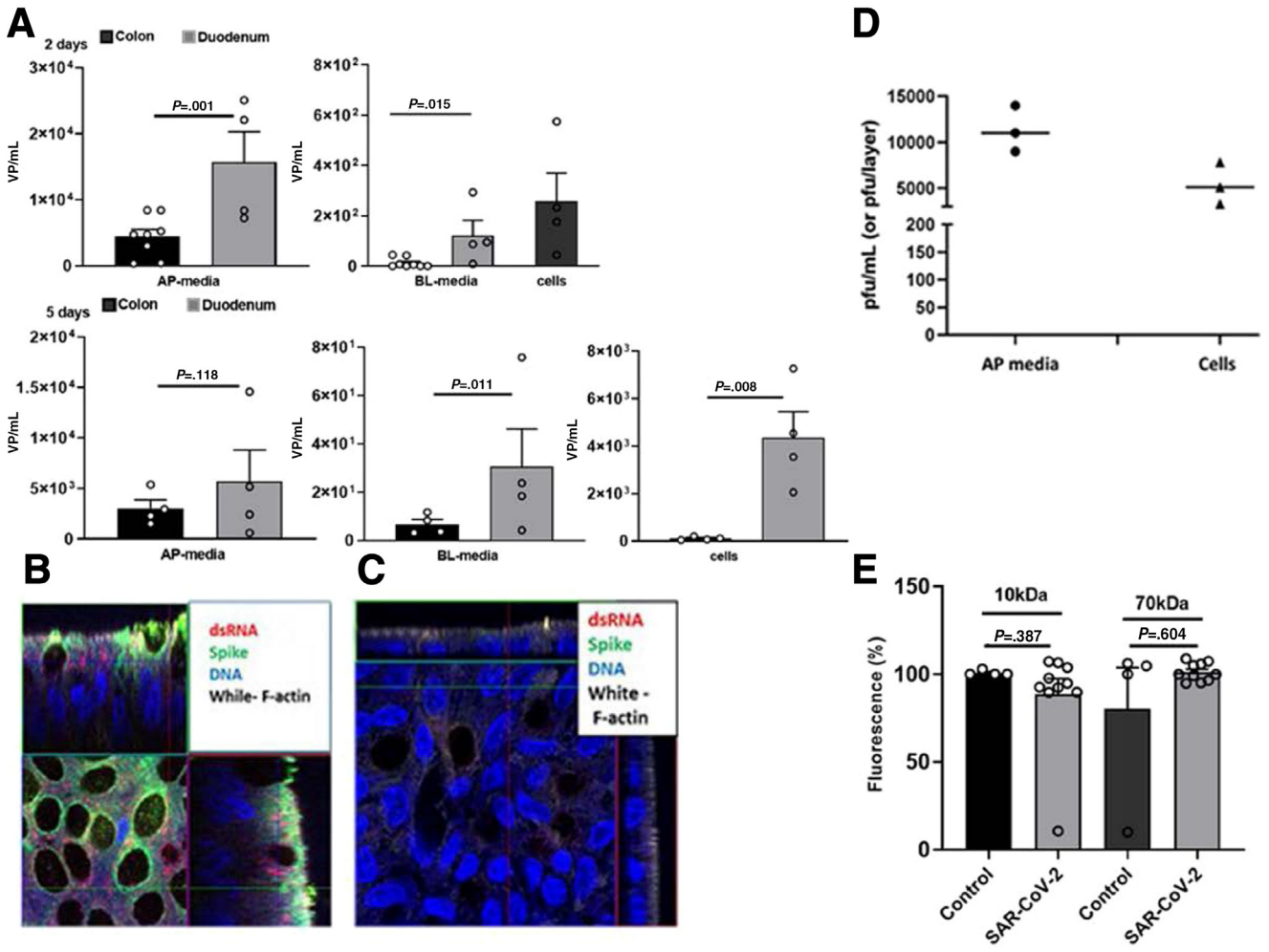

Figure 1. Live SARS-CoV-2 enters and replicates in human enteroid monolayers. (*A*) The apical membrane of differentiated human small intestinal and proximal colonic enteroid monolayers was exposed to live SARS-CoV-2 10^6 PFUs/ml for 90 minutes, then washed to remove virus, and studied for up to 5 days after viral exposure. Apical and BL media from differentiated duodenal or colonoid monolayers and lysates of enterocytes were studied. Total RNA was prepared and expression of viral nucleocapsid was measured by qRT-PCR. The concentration of VPs corresponding to RNA is shown. n = 3. (*B*) Differentiated human colonoid monolayers were treated as in (*A*), and 48 hours later, viral entry was confirmed in colonocytes, using double stranded RNA (dsRNA) antibody (*red*) and viral Spike protein (*green*). This did not occur in goblet cells. (*C*) Spike protein and dsRNA were not detected in uninfected monolayers as a negative control for (*B*). (*D*) Infectious virus was detected in colonoid monolayers as well as in apical media by Vero cell plaque forming assay under conditions in (*A*). Y axis, PFU/ml is for live virus in apical media; PFU/layer is for the cells in monolayer. n = 3. (*E*) Viral infection of differentiated colonoid monolayers did not affect epithelial permeability of fluorescent 10 or 70 kDa dextran when studied 2 days after initial viral exposure. Dextran was added apically, and subsequent BL collection is shown with results normalized to the amount of dextran in untreated conditions set as 100% in each experiment. n = 3. All results are means ± SEM.

Live SARS-CoV-2 Infection Lowers ACE2, NHE3, and DRA mRNAs and NHE3 and DRA Protein Expression but does not Affect CFTR mRNA or Protein Expression

A total of 10^6 PFUs/ml live SARS-CoV-2 was exposed to the apical surface of differentiated human proximal colonic enteroids as described above. mRNAs were then analyzed for the viral receptor ACE2 and several transport proteins known to be involved in the pathogenesis of multiple diarrheal diseases. Forty-eight hours after exposure to live virus, mRNAs for ACE2, NHE3, and DRA were significantly reduced, whereas there was no significant effect on CFTR mRNA (Figure 3*A*). Similar studies measured NHE3, DRA, and CFTR protein expression in ileal enteroid monolayers. Live SARS-CoV-2 significantly reduced NHE3 and DRA but not CFTR protein expression 48 hours after a 90-minute exposure to live virus (Figure 3*B*).

Effect of VLPs With 4 SARS-CoV-2 Structural Proteins on Cytokine Secretion and Also Plus IL-6 and IL-8 on Transporter and ACE2 mRNAs

To determine whether viral replication is necessary for proinflammatory responses and effects on diarrhea-related transport protein expression, and to allow use of

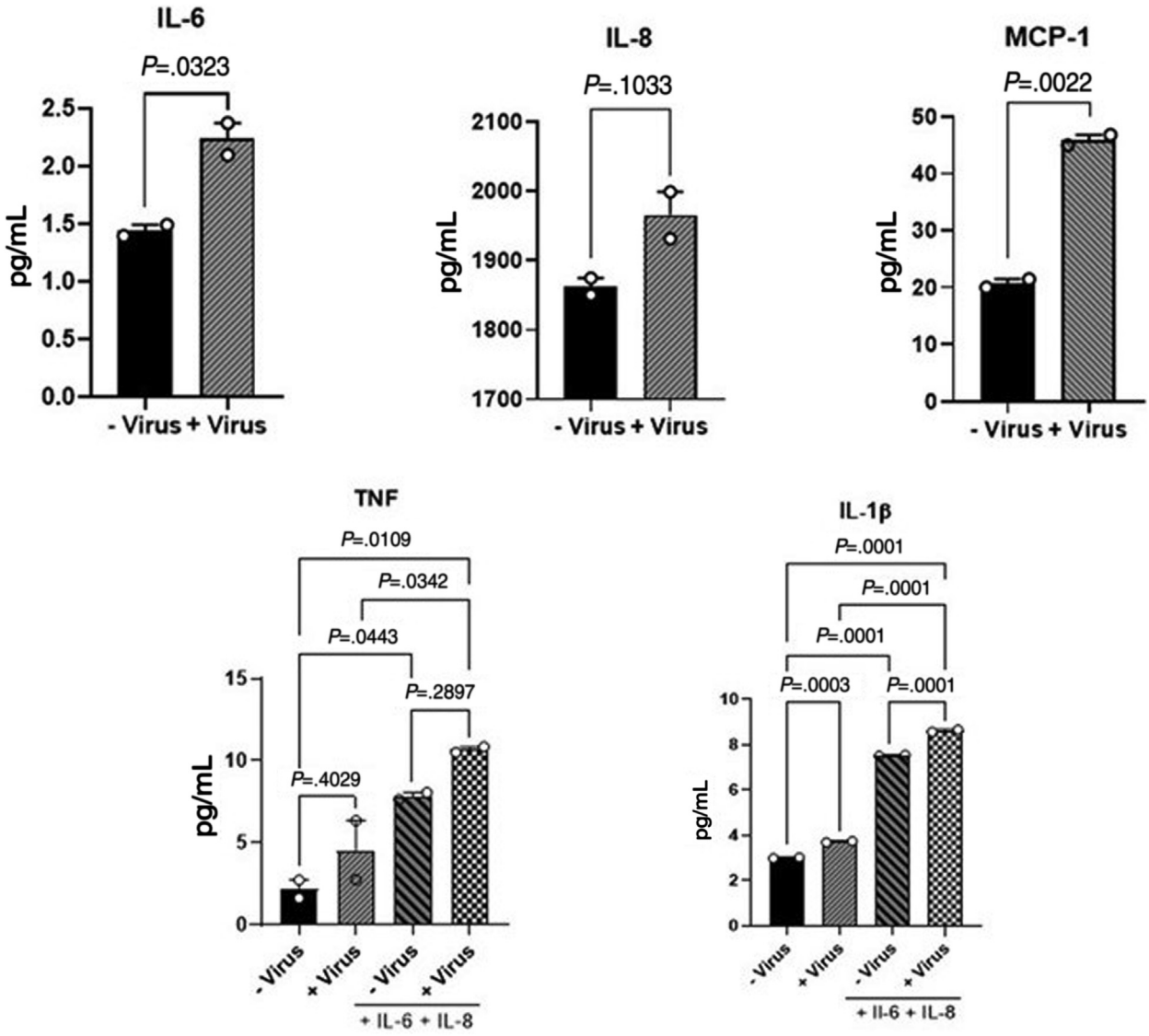

Figure 2. SARS-CoV-2 stimulates epithelial cytokine/ chemokine secretion in human duodenal enteroid monolayers. Differentiated human enteroid monolayers were exposed on the apical surface to SARS-CoV-2 (10^6 PFU/ml) for 90 minutes; the virus was then washed out and evaluated 48 hours after initial exposure. Some studies, as shown, were performed in the presence of IL-6 and IL-8 (50 ng/ml each) on the basolateral surfaces for 48 hours. BL media were collected and analyzed for secreted cytokines/chemokines by multiplex enzyme-linked immunosorbent assay (ELISA). Live virus significantly increased IL-6, MCP-1, and IL-1b. Two separate experiments with triplicate assays in each. Results are means ± SEM.

technology not available for use in our Biosafety Level-3 facilities with live virus, studies were undertaken with exosomes containing the 4 structural SARS-CoV-2 proteins. Having shown SARS-CoV-2 effects on human small intestinal and colonic enteroids, further studies were carried out on human ileal enteroid monolayers. This was based on the similarity of response to live virus of human small intestinal and proximal colonic enteroids and that the highest intestinal amount of ACE2 is in the human ileum. Considering that VLPs did not replicate, the VLPs were added to differentiated ileal enteroid monolayers at times 0 and 24 hours and studied at 48 hours after the initial exposure. The VLPs with Spike D614G bound to the enteroid BB and these VLPs were taken up by the enteroids as indicated by immunofluorescence (IF) (Figure 4*A*). These VLPs, compared with the same concentration of exosomes without SARS-CoV-2 structural proteins, significantly increased basolateral secretion of MCP-1 and caused basolateral increase in IL-6, IL-8, and TNF-α, which did not reach statistical significance (Figure 4*B*).

Similar conditions were used to evaluate the effects of VLPs on ileal enteroid monolayer expression of mRNAs for ACE2, NHE3, DRA, and CFTR. These studies included BL presence of IL-6 and IL-8 (50 ng/ml each) to mimic the conditions produced by live virus and to model the presence of the virus-induced inflammatory response. The VLPs/IL-6, IL-8 significantly reduced the mRNAs for ACE2, NHE3, DRA, and CFTR (Figure 4*C*). We conclude that the VLPs, in spite of

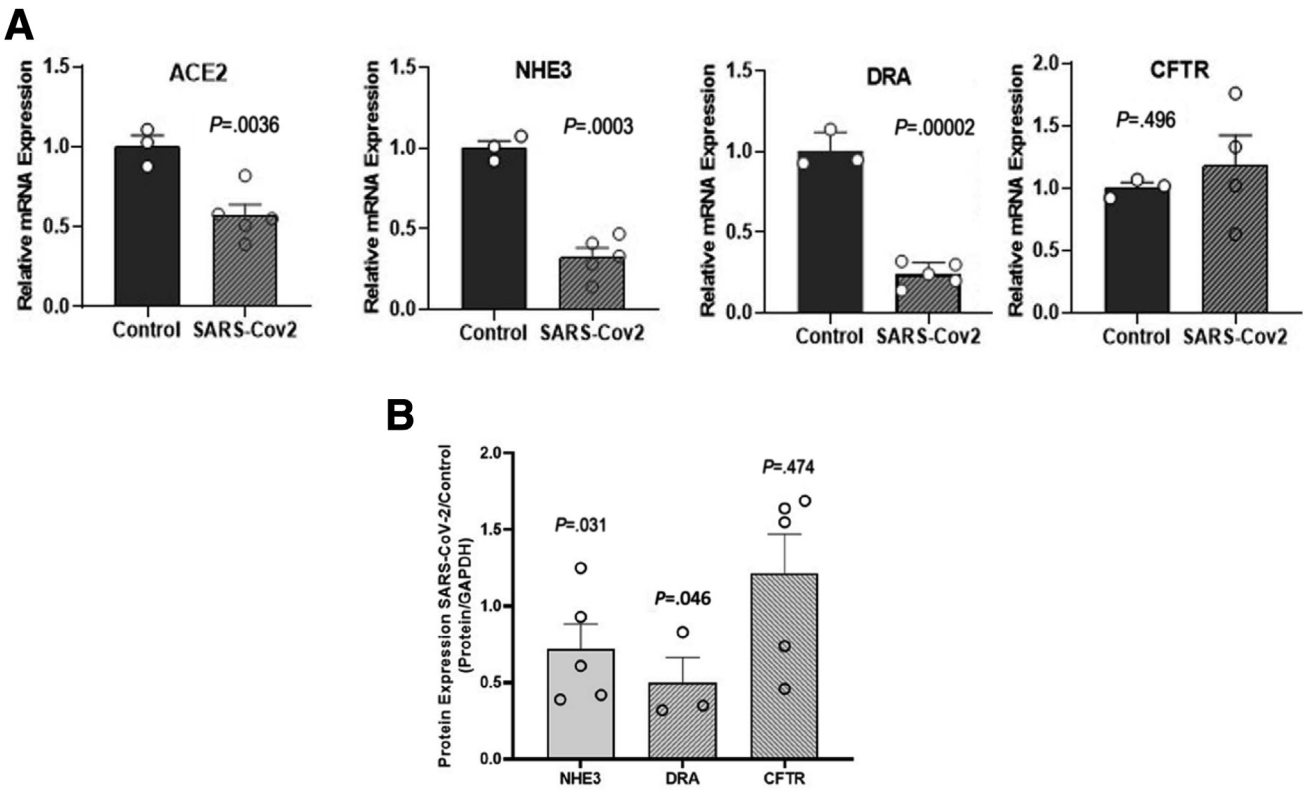

Figure 3. Live SARS-CoV-2 reduces NHE3 and DRA but not CFTR mRNAs and NHE3 and DRA but not CFTR protein expression. (*A*) Effect of SARS-CoV-2 infection on the mRNA expression of ACE2, NHE3, DRA, and CFTR human colonoid monolayers. Live SARS-Cov-2 virus was apically exposed for 90 minutes (10^6 PFU/ml) to proximal colonoid monolayers from 3 different donors and studied at 48 hours. There was reduced mRNAs for ACE2, NHE3, and DRA, but not CFTR. Results are means ± SEM; n = 3–5. Normalization was to S18 ribosomal protein mRNA. (*B*) Effect of SARS-CoV-2 infection on the protein expression of NHE3, DRA, and CFTR in human ileal enteroid monolayers studied as in (*A*) above. Results are means ± SEM. In (*B*), data shown as ratio of paired virus/control monolayers due to wide variation among NHE3, DRA, and CFTR protein/GAPDH ratios. n = 3–5 monolayers. *P* values are comparison with untreated control enteroids; paired *t*-tests.

not having viral RNA replication, duplicated the effects of live virus in terms of uptake into enterocytes, production of cytokines, and, in the presence of IL-6 plus IL-8, mimicked the effects of live virus by reducing mRNAs for ACE2, NHE3, and DRA, although in addition VLPs/IL-6, IL-8 reduced the mRNA of CFTR. The live virus and these VLP/IL-6, IL-8 effects demonstrated that by 48 hours after live virus or VLP exposure plus IL-6 and IL-8, NHE3, which is part of intestinal neutral NaCl, was reduced. DRA mRNA was significantly reduced as was the DRA protein level.

VLPs Plus IL-6 and IL-8 Cause Ileal Anion Secretion

Transport processes affected in many diarrheal diseases include stimulated Cl^- secretion, usually via stimulation of CFTR, in addition to inhibition of NHE3 and DRA. Consequently, the effect of VLPs on active anion secretion measured by the Ussing chamber/voltage clamp technique was studied in undifferentiated ileal enteroids (Figures 5 and 6). Acute apical addition of VLPs alone inconsistently elevated Isc (Figure 5*F*). However, when monolayers were pretreated basolaterally with IL-6 plus IL-8 for ∼18 hours before study to again mimic part of the inflammatory response induced by SARS-CoV-2, apical VLPs caused active anion secretion (Figures 5 and 6). No change in Isc was caused by adding the cytokines alone studied immediately, and the basal Isc was not altered 18 hours after cytokine exposure when compared with untreated ileal monolayers (data not shown). The active anion secretion occurred ∼4 to 12 minutes after VLP addition to IL-6, IL-8 pretreated enteroids (time to onset of increase in Isc was 7.6 ± 2.7 minutes, n = 5 experiments, 9 monolayers), lasted for the time studied up to 40 minutes, and was concentration-dependent with 3×10^8 particles/ml (Figures 5 and 6) but not 1×10^8 or 2×10^8 particles/ml producing a consistent increase in Isc. This increase in Isc was further characterized (Figures 5 and 6), and was fully inhibited by pretreatment with BAPTA-AM (35 uM, 30 minutes) (Figures 5*A* and 6*A*) and reversed by the basolateral addition of the K channel inhibitor, clotrimazole (Figures 5*B* and 6*B*). The CFTR inhibitor BPO-27 did not reverse the VLP-induced increased Isc (Figures 5*B* and 6*D*). In contrast, anion secretion was reversed by the general calcium-activated Cl^- channel (CaCC) inhibitor-Ao1 (Figure 5*C* and *D*; Figure 6*C* and *D*), and partially reversed by pretreatment with the specific TMEM16A inhibitor-Ao1 (Figure 5*E* and Figure 6*F*).

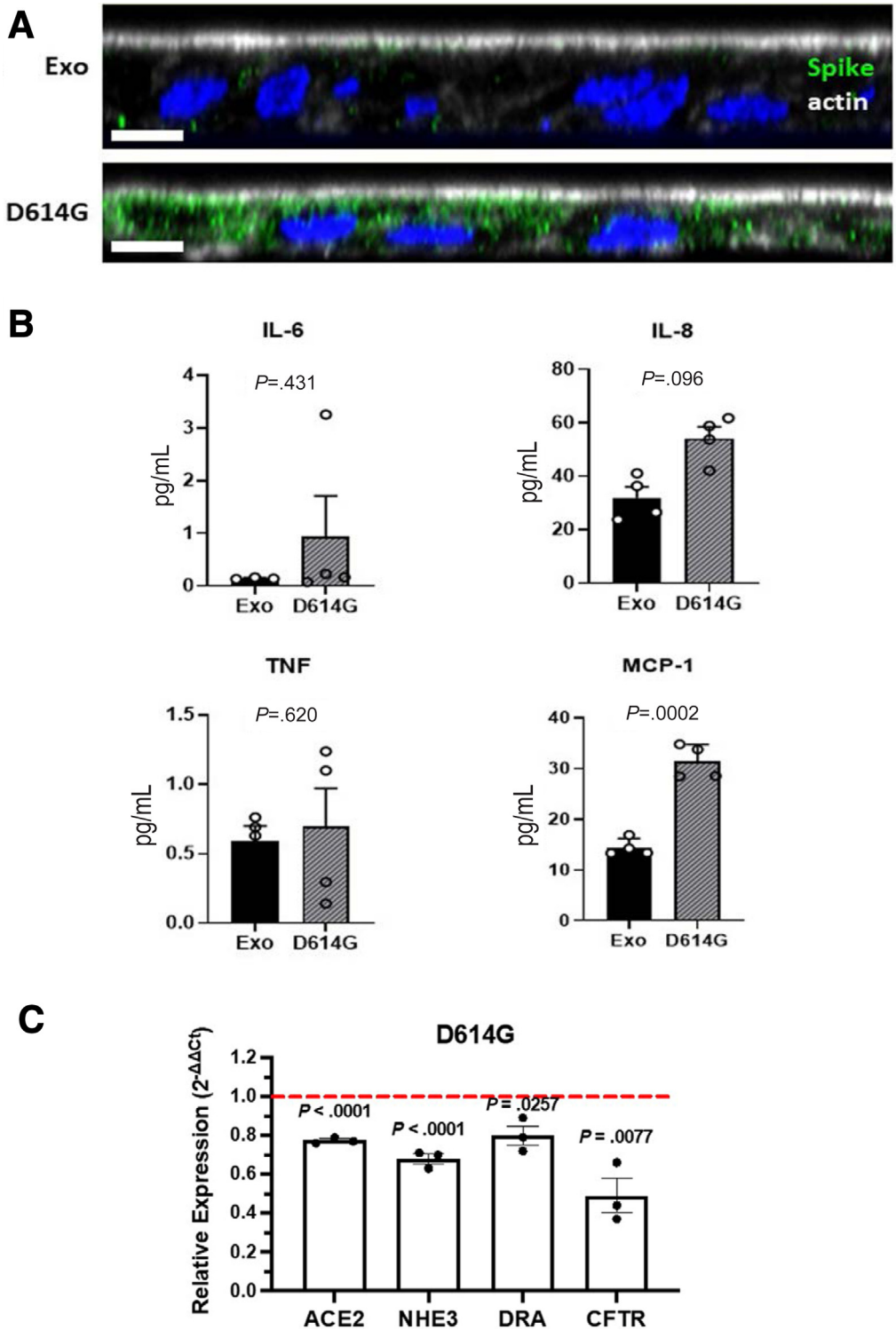

Figure 4. SARS-CoV-2 VLPs directly bind and stimulate cytokine/chemokine secretion in human ileal enteroid monolayers and reduce mRNAs for ACE2, NHE3, DRA, and CFTR. (*A*) IF confocal microscopy (XZ plane shown) demonstrating binding of 10^6 particles/ml VLPs were added at times 0 and 24 hours, and monolayers fixed at 48 hours. Exo = empty exosomes; *green* = anti-rabbit polyclonal antibodies to SARS-COV-2 spike protein; *white* = phalloidin (actin); *blue* = Hoechst 33342 (nuclei). Scale bar, 10 um. Similar results of experiments repeated twice. (*B*) Differentiated human ileal enteroid monolayers were apically exposed to empty exosomes (Exo) or 10^6 particles/ml SARS-CoV-2 VLPs, added as in (*A*) at times 0 and 24 hours and sampled at 48 hoours. BL media were collected and analyzed for secreted cytokines/chemokines by multiplex enzyme-linked immunosorbent assay (ELISA). (*C*) VLPs expressing the 4 SARS-CoV-2 structural proteins, including Spike D614G, were exposed apically to ileal enteroid monolayers as in (*B*) and studied at 48 hours, with IL-6 and IL-8 (50 ng/ml each) on the BL surface. Effects on mRNAs demonstrated that, compared with exosomes similarly exposed, there was significant reduction in ACE2, NHE3, DRA, and CFTR. Data shown are normalized to effect of empty exosome controls set as 1.0 for each experiment (horizontal line). Results are means ± SEM. n = 3.

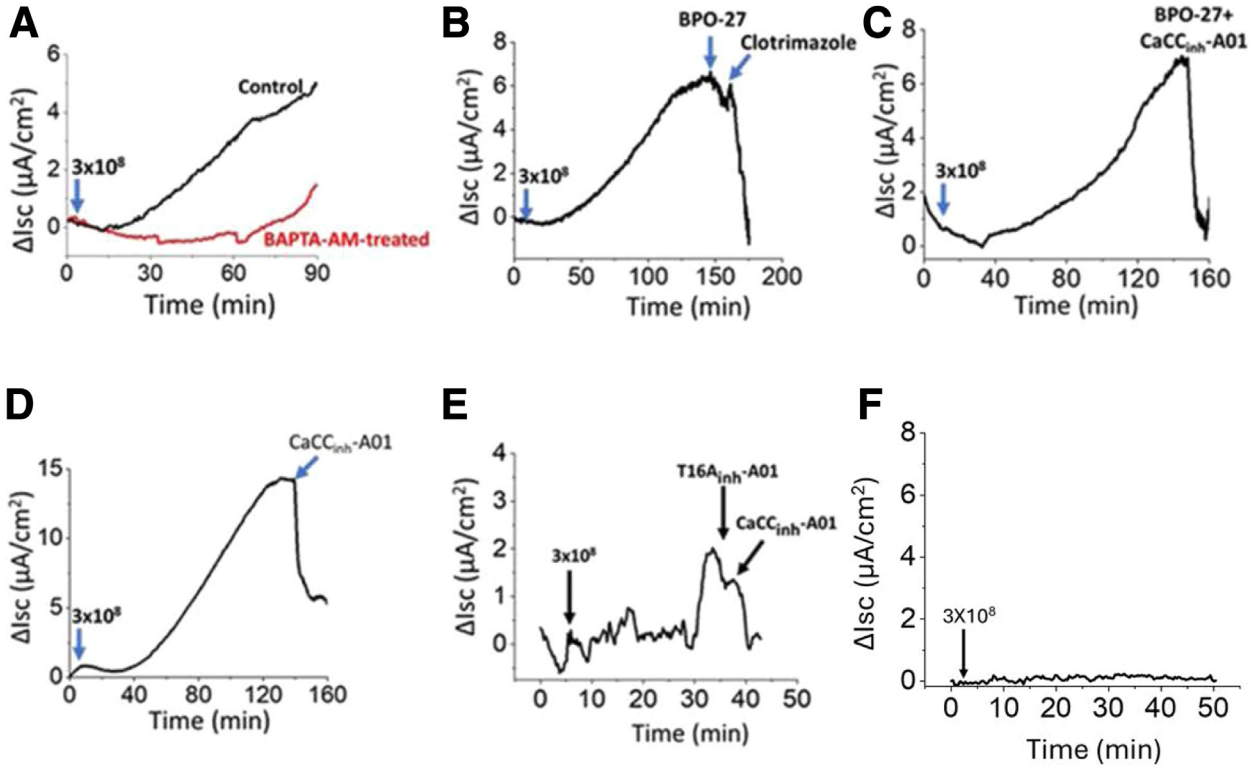

Figure 5. VLPs plus IL-6 and IL-8 cause active anion secretion in human ileal enteroids. Ussing chamber/voltage clamp studies of active electrogenic ion transport were performed in the presence of IL-6 plus IL-8 (both 50 ng/ml added basolaterally ~18 before study). Arrows show time of VLP addition. Three × 10^8 VLPs/IL-6, IL-8 stimulated an increase in Isc which began 4 to 20 minutes after VLP addition. The increase in Isc occurred in 21 of 23 monolayers exposed to the VLPs. The increase in Isc (*A*) was prevented by pretreatment by BAPTA-AM (35 uM, 30-minute pretreatment); (*B*) Reversed by BL exposure to the K channel inhibitor clotrimazole (30 uM); (*C and D*) Not affected by the CFTR inhibitor BPO-27 (1 μM) but reversed by the CaCC inhibitor- Ao1 (25 μM); and (*E*) Partially reversed by the specific TMEM16A inhibitor- Ao1 (20 uM). All studies shown are of single monolayers. Figure 6 shows these studies as means ± SEM of a series of experiments. (*F*) Representative trace of 5 similar experiments showing lack of effect on Isc of VLP 3 × 10^6 added as in (*A–E*) but without pretreatment with IL-6 plus IL-8.

To further validate that the VLP-induced increase in Isc did not involve CFTR, studies between normal ileal enteroid monolayers and those from a homozygous FΔ508 patient with cystic fibrosis were compared. The VLP/IL-6, IL-8 increase in Isc was similar in both a normal ileal enteroid (organoid 46I) and a CF (homozygous FΔ508) ileal enteroid (CF-U3), and the changes in the increase in Isc were similarly inhibited by sequential TMEM16A and general CaCC inhibitors (Figure 6*E* and *F*). Thus VLPs in the presence but not absence of IL-6, IL-8 causes active anion secretion, which is delayed in onset by minutes, is Ca^+-dependent, and is reversed by both an apical general TMEM16 inhibitor (fully inhibited) and a specific TMEM16A inhibitor (partially inhibited) but is not reversed by a CFTR inhibitor.

Enteroid Effects of Irradiated SARS-CoV-2

Irradiated SARS-CoV-2 was studied as another way to evaluate virus effects in the absence of viral replication. Because live SARS-CoV-2 and VLPs both entered enterocytes and induced an inflammatory response, studies were undertaken to attempt to separate direct effects of viral infection and induction of cytokine release. Differentiated human ileal enteroid monolayers were apically exposed to the same virus used for the live viral studies but that had been irradiated, making the virus replication deficient.[22] A total of 10^6 VPs/ml were exposed apically, and presence within the enteroids determined at several times by immunoblotting enteroid lysates with anti-Spike antibody. Spike was present at 2 and 4 hours after exposure but not at 24 hours, consistent with failure to replicate (Figure 7). To define the effect of irradiated virus on enteroid production of cytokines, 10^6 VPs/ml were exposed apically to differentiated human ileal enteroid monolayers at time 0 and 24 hours and sampled at 48 hours. Figure 8 shows that irradiated virus did not alter the cytokines, chemokine measured in the basolateral media compared with simultaneously studied untreated control enteroids.

Given the lack of effect of irradiated virus to significantly affect the panel of cytokines secreted in response to live virus, we hypothesized that irradiated virus would also not alter expression of NHE3 and DRA. Human ileal enteroid monolayers were exposed to $10^{6\text{-}8}$ VP/ml over 48 hours, by addition of irradiated virus at time 0 and 24 hours, and effects were determined on enteroid mRNAs (NHE3, DRA, CFTR, TMEM16A, TMEM16F) and NHE3 protein expression at 48 hours. These effects were compared with the effects

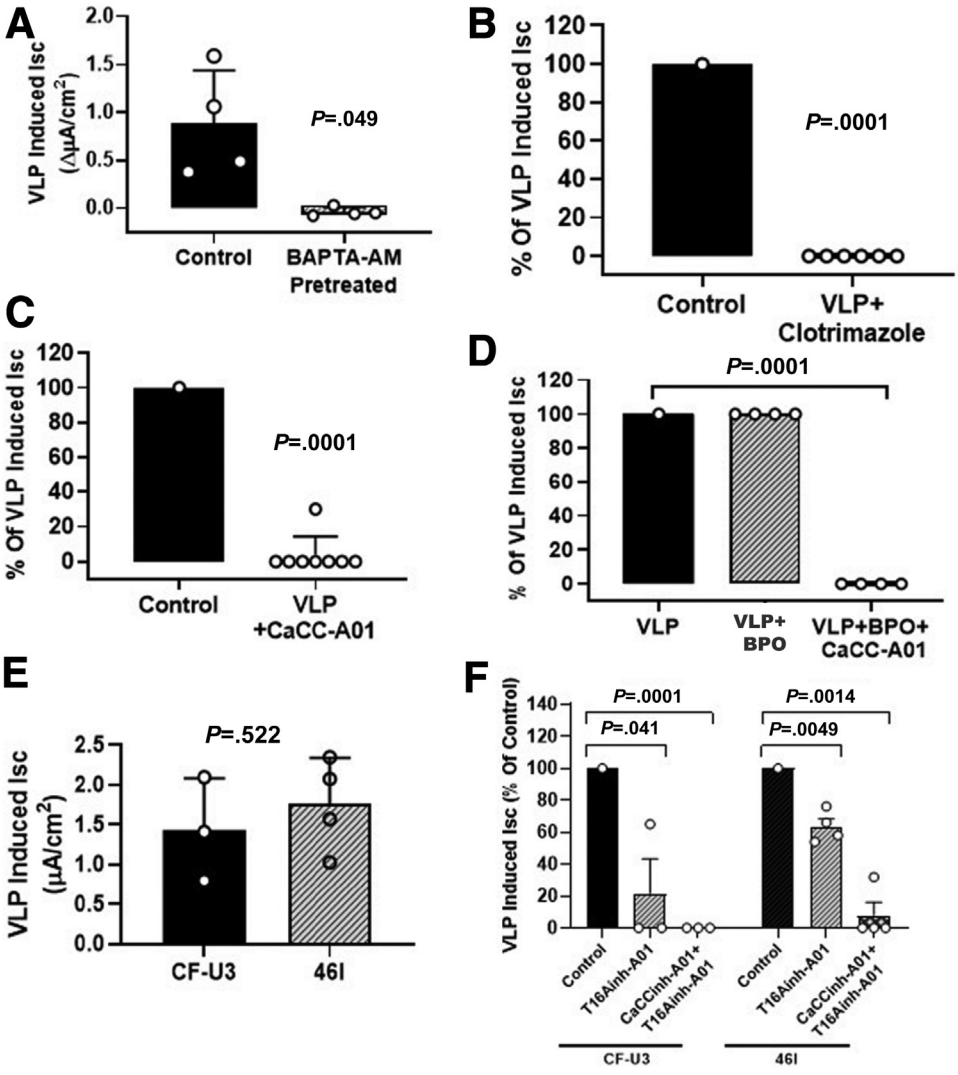

Figure 6. VLPs plus IL-6 and IL-8 cause active anion secretion in human ileal enteroids. Effects of apical VLPs/IL-6, IL-8 on ileal Isc: (*A*) BAPTA-AM; (*B*) Clotrimazole; (*C*) BPO-27; (*C and D*) CaCC inh-Ao1; (*E*) Comparison of Isc increase caused by VLP/IL-6, IL-8 in normal ileal enteroids (name of ileal enteroid is 46i) and human homozygous FD508 ileal enteroids (CF ileal enteroid CF-U3); (*F*) Effect of $TMEM16A_{inh}$-Ao1 and general $CaCC_{inh-}$ Ao1 on increase in Isc caused by VLP/IL-6, IL-8 on normal ileal enteroids and human homozygous FD508 ileal enteroids. Results are means ± SEM; n = 3–7.

of addition of IL-6 plus IL-8 (50 ng/ml each) both added at time 0 to the basolateral surface of enteroids, and to the combination of irradiated virus plus IL-6, IL-8 and to untreated controls (Figure 7). Irradiated virus did not significantly reduce the mRNAs for any of the genes studied, and, in fact, the DRA mRNA was increased; in contrast, IL-6 plus IL-8 alone reduced expression of NHE3 and DRA, while not significantly affecting expression of CFTR, TMEM16A, or TMEM16F. The effect of IL-6 plus IL-8 plus irradiated virus was not different from the effect of IL-6 plus IL-8 alone.

In parallel to the mRNA studies, IB and IF studies of differentiated human ileal enteroid monolayers were examined for NHE3 expression. Exposure to irradiated virus (10^6 VP/ml added at time 0 and 24 hours and examined at 48 hours after initial viral exposure), did not alter NHE3 expression (Figure 7*D, left*). In contrast, exposure to IL-6 plus IL-8 reduced total expression of NHE3 (Figure 7*D, right*). Thus 48 hours of exposure to IL-6 plus IL-8 mimics the effect of intact virus to inhibit mRNAs of NHE3 and DRA and also to reduce the expression of NHE3 protein, whereas irradiated virus did not alter mRNA expression of NHE3 and DRA or NHE3 protein expression.

Mechanism of Stimulated Anion Secretion by Human Enteroids: Induction of Ca^{2+} Waves

Mechanistic studies to further define how SARS-CoV-2 acutely stimulated anion secretion concentrated on the potential role of intracellular Ca^{2+}, given the BAPTA-AM inhibition of the anion secretion and the dependence of the anion secretion on CaCCs in comparison to the lack of contribution of CFTR. The effects of irradiated virus and VLPs were determined and compared with the effect of IL-6 plus IL-8 on intracellular Ca^{2+} in human ileal enteroids stably expressing the Ca^{2+} sensor GCamP-6s. Extensive labeling of ileal enteroids stably expressing lentivirus-GCamP-6s was achieved by selection with puromycin (Figure 8*A*). Intracellular Ca^{2+} was quantitated using confocal microscope images processed by Metamorph software (excitation

488 nm, emission 500-580 nm). Because undifferentiated enteroids model intestinal Cl^- secreting crypts, studies were performed with undifferentiated monolayers. Effects on intracellular Ca^{2+} of VLPs and irradiated virus were similar (Figures 8 and 9; Movie). Addition of 10^8/ml VLPs or irradiated virus apically caused a rapid onset of Ca^{2+} waves which usually started ~5 to 10 minutes after VLP exposure. By examining the sites at which Ca^{2+} elevation first occurred, the elevation was found to arise from a small group of cells. Ca^{2+} waves were defined as Ca^{2+} elevations that spread from a single cell or small groups of cells that involved at least 3 to 5 cells. In the absence of VLPs or irradiated virus or only with empty exosomes (10^8/ml) as a control for the VLP studies, some spontaneous Ca^{2+} waves occurred (Figures 8 and 9; Movie). The VLP and irradiated virus exposure increased the number of Ca^{2+} waves and also the total magnitude (number of summed pixels) of the Ca^{2+} waves (Figure 8*B* and *C* and Figure 9*A* and *B*).

Once initiated, the Ca^{2+} wave response in ileal enteroids persisted for the 60-minute period over which most studies

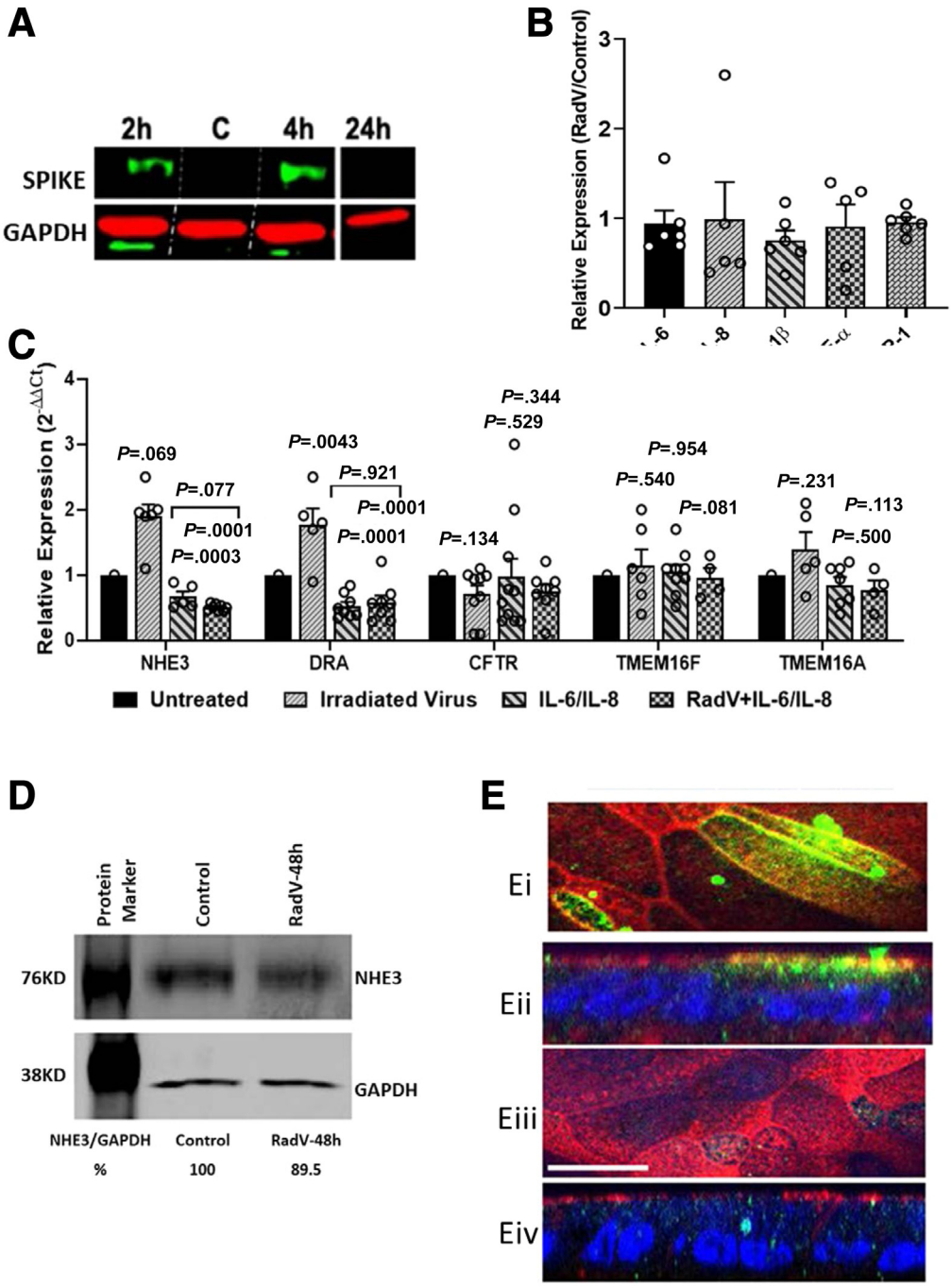

were carried out. In several instances, the monolayers were followed overnight with some continuation of the Ca^{2+} waves for at least 14 hours. To illustrate the part of the ileal enteroid monolayers in which the Ca^{2+} waves occurred, the 60-minute time series following the Ca^{2+} levels was compressed into a single maximum intensity projection, and areas in which Ca^{2+} waves occurred were manually marked and waves appearing at the same time shown in the same color. This demonstrated that Ca^{2+} waves occurred in many areas at many different times with some of the areas experiencing multiple Ca^{2+} waves over 1 hour (Figure 9*C*). The VLP and irradiated virus-induced Ca^{2+} waves were spread over the entire field of view.

In contrast to the VLP and irradiated virus, both of which stimulated Ca^{2+} waves, the effect of IL-6 plus IL-8 (50 ng/ml) exposed to the ileal enteroids ~18 hours before virus exposure or acute addition did not alter basal Ca^{2+} in absence of virus addition and did not alter the overall Ca^{2+} waves caused by virus addition (shown for irradiated virus, Figure 8*B–D*). This indicated that induction of the Ca^{2+} waves was not an inflammation-dependent process. The effect of several antagonists on the Ca^{2+} waves was determined over the first hour after irradiated virus and VLP exposure. These antagonists were selected to compare effects in Ca^{2+} elevation and in VLP-induced stimulation of Cl^- secretion in the ileal enteroids. Significant inhibition of the number of Ca^{2+} waves and the magnitude of the waves that occurred in the first hour was detected with pretreatment with the general CaCC inhibitor, $CaCC_{inh}$-Ao1 (20 uM, pretreatment 30 minutes), the P2Y1 receptor antagonist BPTU (5 uM, pretreatment 60 minutes), and apical apyrase, an enzyme that breaks down ATP and ADP. Importantly, the TMEM16A inhibitor, TME16Ainh-Ao1 (20 uM, pretreatment 30 minutes) did not alter the irradiated virus or VLP stimulation of ileal enteroid Ca^{2+} waves (Figure 8*B* and *C*; Figure 9*A–C*). This indicates that TMEM16 family member(s) are involved in the virus stimulated increase in intracellular Ca^{2+}, but TMEM16A is not the isoform involved.

Discussion

This mechanistic study has defined multiple aspects of the pathophysiology of the diarrhea that occurs commonly as part of acute COVID-19. Based on a model that uses human intestinal enteroids from multiple intestinal segments, COVID-19 diarrhea has unique features, although it has similarities with other acute diarrheal diseases in that it occurs with inhibition of intestinal Na^+ absorption (via changes in the neutral NaCl absorptive process with both NHE3 and the linked DRA reduced) and stimulation of active electrogenic anion secretion.[20,21] The unique aspects of this diarrhea appears to be that it is inflammatory, includes Cl^- secretion that does not involve CFTR, acts via and requires induction of Ca^{2+} waves, and involves a direct effect of the virus on the intestine in addition to a major contribution of the virus-induced inflammatory state. The findings in this model of COVID-19 were similarly caused by live SARS-CoV-2 and VLPs expressing the 4 SARS-CoV-2 structural proteins plus addition of components of the virus-induced inflammatory response. This suggests that COVID-19 diarrhea is largely due to a combination of the SARS-CoV-2 structural proteins plus the virus-induced inflammatory response from intestinal epithelial cells.

COVID-19 is known not only to be associated with initiation of a cytokine inflammatory response, but also that this drives many of the significant manifestations of the disease, including the devastating respiratory compromise. The current study demonstrated that the inflammatory response (modeled by addition of IL-6 plus IL-8 at an high concentration chosen to mimic the contribution of the systemic inflammatory response) coming in part from the intestinal epithelial cells was a necessary component of the reduced Na^+ absorption and stimulated Cl^- secretion in this model of COVID-19 diarrhea, accounting for (1) the entire reduction in neutral NaCl absorption; and (2) being necessary for acute stimulation of active electrogenic anion secretion along with the elevated intracellular Ca^{2+}. It is important to also note which aspect of the diarrhea

Figure 7. Irradiated virus is taken up in human colonic enteroid monolayers but does not alter enterocyte cytokine secretion or mRNAs of NHE3, DRA, CFTR, TMEM16F, and TMEM16, whereas IL-6 plus IL-8 reduce mRNAs of NHE3 and DRA. (*A*) 10^6 viral particles/ml of irradiated virus were exposed apically to differentiated human enteroid monolayers for various times and intracellular virus identified by IB using anti-Spike antibodies. Representative study, repeated 4 times, is shown. Uptaken Spike is present at 2 and 4 but not 24 hours after exposure. (*B*) Irradiated virus exposure for 48 hours did not alter cytokines/chemokine secretion from differentiated ileal enteroid monolyes. 10^6 PFU/ml irradiated virus was added apically at times 0 and 24 hours to ileal enteroid monolayers and BL media sampled at 48 hours for cytokines and chemokine assays. In parallel, enteroids that were not treated were used as controls. Data shown set the untreated controls as 1 for each experiment. Two separate ileal enteroid lines were studied. Results are means ± SEM; n = 6. (*C*) IL-6/IL-8 but not irradiated virus decreased mRNAs of NHE3 and DRA but not CFTR, TMEM16A, or TMEM16F. Differentiated ileal enteroid monolayers from 3 separate ileal enteroid cultures were exposed on the apical surface to 10^6 PFU/ml irradiated virus, the combination of irradiated virus with IL-6/IL-8 (50 nl/ml each) on the BL surface, or the IL-6/IL-8 alone. Irradiated virus was added at times 0 and 24 hours and IL-6/IL-8 at time 0 and all sampled at 48 hours for mRNA determinations. Results are means ± SEM; n = 4–9. ANOVA used to calculate *P* values shown above bars. Bracketed *P* values compare IL-6/IL-8 effect to combination of irradiated virus plus IL-6/IL-8. (*D*) Irradiated virus exposure for 48 hours did not alter NHE3 protein expression (*left*), but IL-6 plus IL-8 for this time reduced NHE3 (*right*). Three × 10^6/ml irradiated virus was exposed apically at times 0 and 24 hours to ileal enteroid monolayers to IL-6/IL-8 (50 ng/ml each) added at time 0 to the BL surface, and 48 after initial exposure, the entroids were lysed for IB or fixed for IF study of NHE3. Irradiated virus alone did not alter NHE3 protein expression by IB (*left*). *Right*: representative confocal XY images at the level of the the BB (*Ei, Eiii*) and XZ sections (*Eii, Eiv*). *Ei, Eii,* untreated controls; *Eiii, Eiv,* irradiated virus. NHE3, *green*; F-actin, *red*; nuclei, *blue*. IL-6/IL-8 greatly reduced total NHE3 protein expression. Scale bar, 20 um. Experiment on *left* was done once, and those on *right* were repeated 3 times.

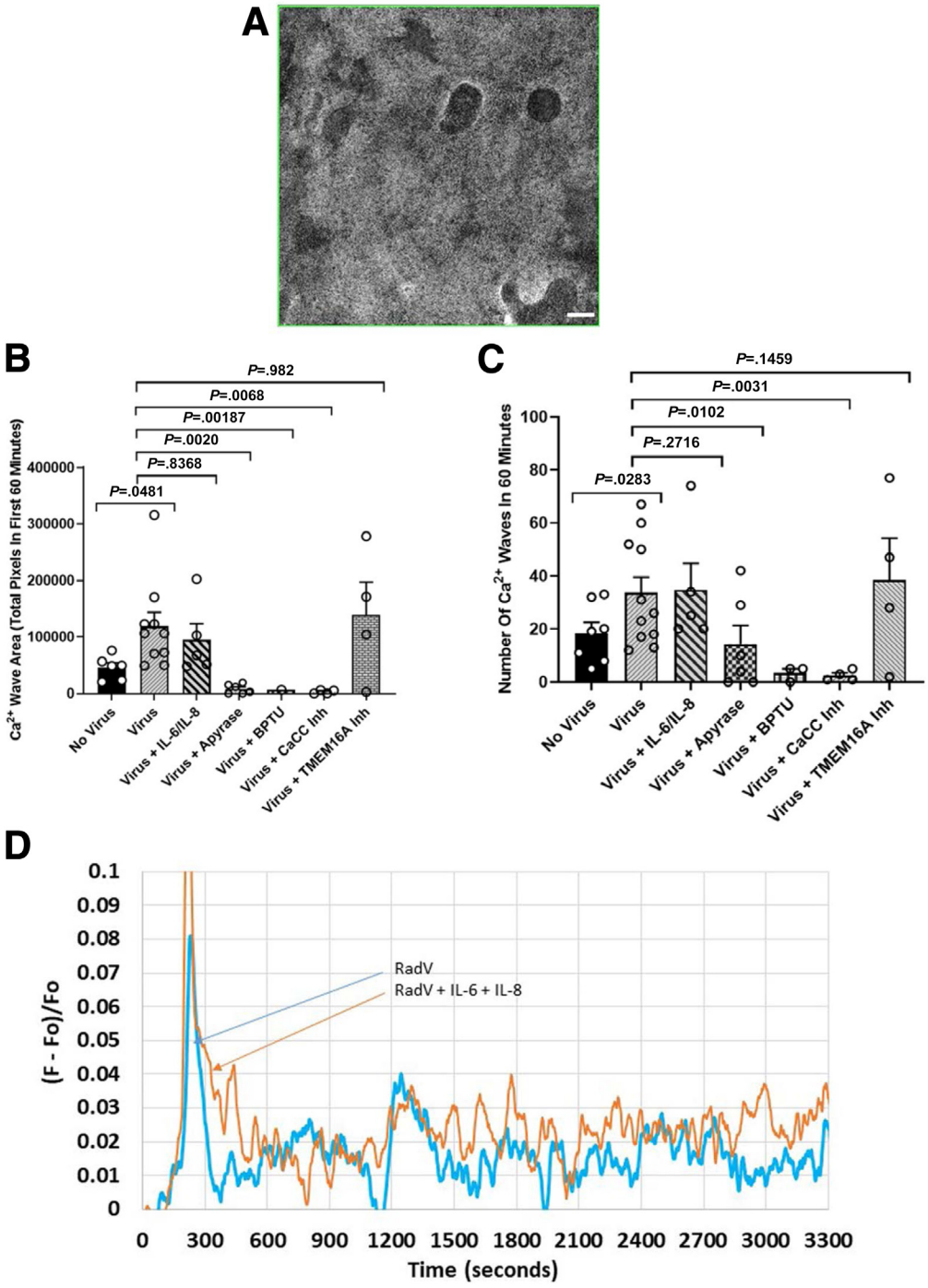

Figure 8. Irradiated virus but not IL-6 plus IL-8 induce Ca^{2+} waves in ileal enteroids. (*A*) IF image of undifferentiated ileal enteroids stably expressing GCamP-6s. This image at excitation 488 nm and emission 500–580 nm was after exposure to 1 uM ionomycin. Scale bar, 5 um. (*B*) Irradiated virus stimulation of ileal Ca^{2+} waves (total Ca^{2+} wave signal). The total pixel counts in these waves is shown. Studies were also performed with pretreatment with IL-6 plus IL-8 (both 50 ng/ml) 18 hours before study, after pretreatment with apyrase, BPTU, the general CaCC inhibitor-Ao1, or the specific TMEM16A inhibitor-Ao1. ANOVA was used to calculate *P* values comparing total Ca^{2+} wave signal to results with irradiated virus. n = 2–10. (*C*) Irradiated virus stimulation of ileal Ca^{2+} waves (total number of waves). Studies were performed with pretreatment with IL-6 plus IL-8 18 hours before study, after pretreatment with apyrase, BPTU, the general CaCC inhibitor-Ao1, or the specific TMEM16A inhibitor-Ao1. ANOVA was used to calculate *P* values comparing total Ca^{2+} wave signal to results with irradiated virus. n = 2–10. (*D*) Ca^{2+} waves in ileal enteroid monolayers illustrated as changes in F-Fo/Fo over 60 minutes comparing effect of irradiated virus with and without pretreatment 18 hours earlier with IL-6 plus IL-8 (both 50 ng/nl). Single experiments from those shown in Figure 8 (*B and C*).

pathogenesis did not involve the SARS-CoV-2 initiated inflammation; the inflammatory state was not involved in the acute intracellular Ca^{2+} elevation, which was necessary for the demonstrated active anion secretion. Of note, however, is that our model with basolateral exposure of our enteroids to IL-6 plus IL-8 mimicked only a small component of the inflammatory response known to be present in COVID-19. These cytokines were selected given their established role in the COVID-19 inflammatory response and our demonstration that they were part of the epithelial response to intestinal SARS-CoV-2 infection.[23–28] In COVID-19 diarrhea, the intestine is almost certainly exposed not only to inflammatory mediators released by the epithelial cells, but also from systemically elevated cytokines plus the contribution from the effect of the virus on the normally present inflammatory cells in the intestinal lamina propria. The latter are probably engaged by the epithelial initiated cytokine response and potential transcellular movement of the virus from infected epithelial cells. This was illustrated in our studies by the significantly increased TNF-α and IL-1β secreted from the enteroids when initially exposed to IL-6 and IL-8 plus SARS-CoV-2. Although COVID-19 diarrhea is generally not life-threatening, this identification of the importance of the inflammatory response suggests testing the role of inhibitors of this response as a way to treat the diarrhea: not only the acute diarrhea but also the diarrhea that occurs in $\sim$30% of patients with long COVID. Until now, no clinical data has been presented of the effect on COVID-19-related diarrhea of modifying the inflammatory response.

The direct role of SARS-CoV-2 in the pathogenesis of diarrhea, in addition to initiating the inflammatory response, is its necessary role in acutely stimulated anion secretion that occurred with VLP exposure. In these anion secretory studies, IL-6 plus IL-8 addition was required to allow mimicking the effect of live virus, since the acuteness of the assay did not allow time for significant accumulation of the cytokines induced by the VLPs. Not further defined, however, was which aspects of the pathogenesis contributed by the direct viral effects could be attributed to one of the 4 structural proteins expressed in the VLPs, beyond the necessity of Spike binding. However, we demonstrated that VLPs containing a mutant of Spike that bound but did not enter the enterocytes did not cause consistent anion secretion studied under the same conditions used for the VLPs in the current study.[29] The failure of irradiated virus to duplicate all effects of both live virus and the VLPs was not further explored, and the irradiated virus did mimic the induction of the Ca^{2+} waves caused by the VLPs. Although it is likely that the radiation damaged SARS-CoV-2 proteins to cause its failure to induce anion secretion and initiate cytokine secretion, its study was useful in allowing separation of direct viral effects vs effects of virus induced inflammation on NHE3 and DRA expression and in demonstrating that elevation of virus-induced elevation of intracellular Ca^{2+} waves was necessary but not sufficient for causing active anion secretion.

An unusual aspect of the pathogenesis of COVID-19 diarrhea is that the electrogenic anion secretion does not appear to involve CFTR and rather was dependent on TMEM16A and other TMEM16 family members. We showed that live SARS-CoV-2 exposure did not alter CFTR transcription (Figure 3). Importantly, relating to demonstration of active anion secretion by VLP/IL-6 and IL-8, not only did the CFTR inhibitor BPO-27 fail to alter the VLP/IL-6 and IL-8 stimulated anion secretion, but the stimulated anion secretion was similar in magnitude in ileal enteroids from normal subjects and from a patient with cystic fibrosis due to a homozygous FΔ508 mutation. Moreover, the inhibition of the stimulated anion secretion by the general TMEM16 family inhibitor (near total inhibition) and that of the specific TMEM16A inhibitor (partial inhibition) were also similar in the normal and cystic fibrosis enteroids (Figure 6). The involvement of TMEM16A, potentially in stimulation of Cl^- secretion, is further supported by the lack of effect in altering the VLP-induced elevation of intracellular Ca^{2+} by a specific TMEM16A inhibitor, while this inhibitor did partially reverse the VLP-induced increase in Isc. However, understanding how TMEM16A is involved in the stimulated anion secretion must consider that its cellular localization has not been established (suggested as being entirely intracellular or on or near the basolateral membrane or on the BB), nor is it role in any intestinal Cl^- secretory process clear (for instance, why is appears to be necessary for CFTR function, or how to consider its reported effects on intestinal cells that are non-enterocytes).[30–38]

Elevation in enteroid intracellular Ca^{2+} that resulted from a direct SARS-CoV-2 effect (IL-6 plus IL-8 did not elevate Ca^{2+} or further increase the intracellular Ca^{2+} level above that caused by the irradiated virus) is a second messenger involved in the SARS-CoV-2-induced active anion secretion. Evidence that Ca^{2+} elevation was necessary for the SARS-CoV-2 (VLP) stimulation of anion secretin, included: (1) BAPTA-AM pretreatment prevented the anion secretion; (2) timing of VLP stimulation of anion secretion and initiation of Ca^{2+} waves were similar; and (3) general CaCC inhibitor blocked both Ca^{2+} elevation and anion secretion.

The elevation in intracellular Ca^{2+} involved Ca^{2+} waves that were initiated within minutes of VLP exposure. That these were waves was supported by tracing the wave back temporally to initiation from very few cells. Most of the waves that occurred over the 60 minutes of observation after VLP addition occurred in separate areas of the monolayer, although in multiple cases, the same areas exhibited multiple waves. Our attempt to further define characteristics of the Ca^{2+} waves, including whether the Ca^{2+} source involved entry of extracellular Ca^{2+}, failed technically, as extracellular EGTA rapidly caused the cells to fall off the monolayers. We had previously reported VLP induction of Ca^{2+} elevation in Caco-2 cells.[29] Although there are no reports of elevation of intracellular Ca^{2+} in pathogenesis of most other aspects of COVID-19, HEK 293 cells exposed to a pseudovirus with SARS-CoV-2 Spike elevated intracellular Ca^{2+}[38]; of interest was that there was a several minute delay after this pseudovirus exposure in onset of Ca^{2+} elevation, as occurred in response to VLPs in our studies. This increase in HEK cell Ca^{2+} was inhibited by a serine protease inhibitor that inhibited TMPRSS2 cleavage

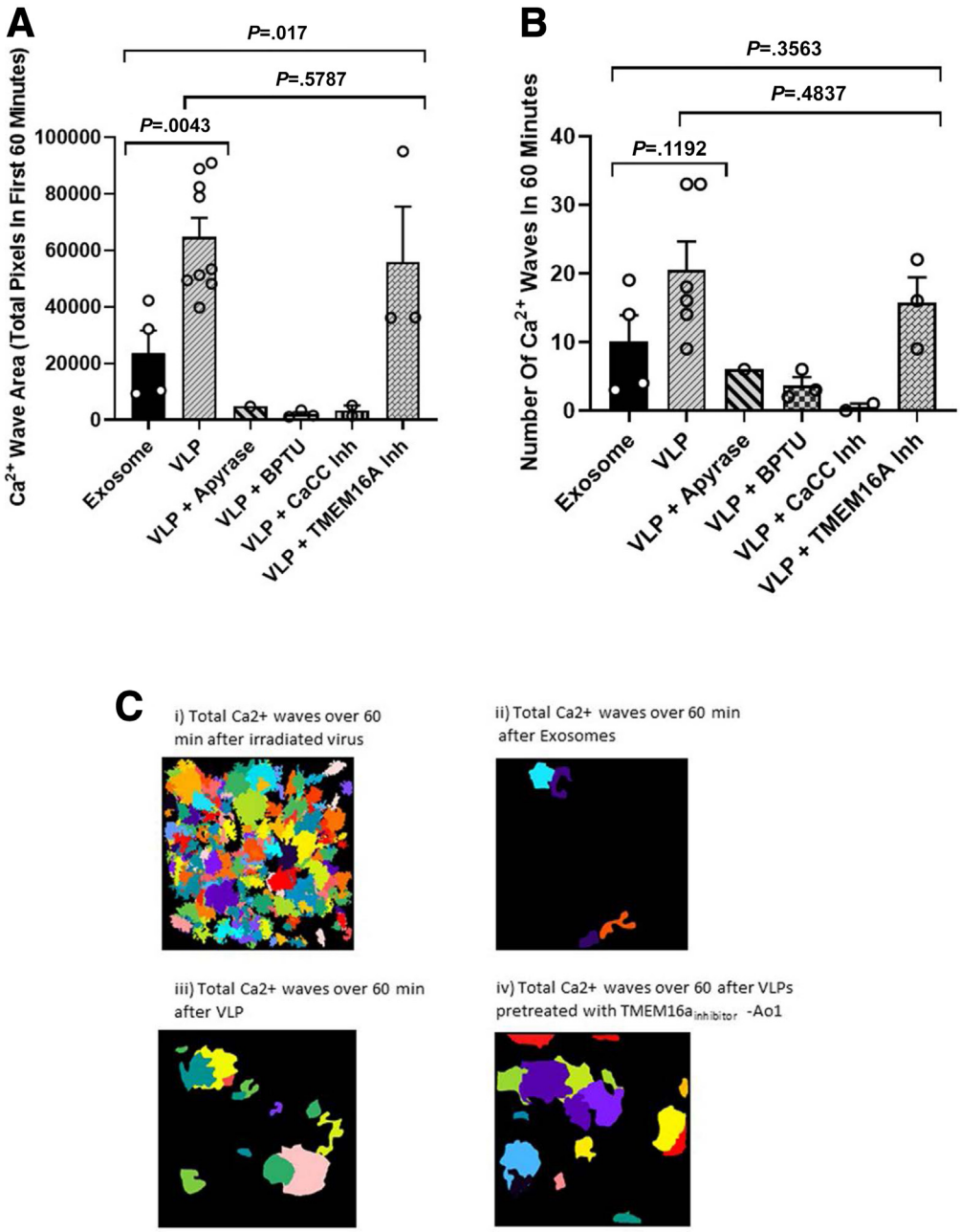

Figure 9. VLP stimulation of ileal Ca^{2+} waves. (*A*) Ca^{2+} waves (total signal in pixels) induced by VLPs and effects on the signal by pretreatment with apyrase, BPTU, the general CaCC inhibitor-Ao1, or the specific TMEM16A inhibitor-Ao1 with exosome controls. ANOVA used for statistical evaluation. n = 3–9. (*B*) Ca^{2+} waves (total number of waves) induced by VLPs and effects on the signal by pretreatment with BPTU, CaCC inhibitor-Ao1, or TMEM16A inhibitor-Ao1 with exosome controls. ANOVA used for statistical evaluation. n = 3–9. (*C*) Pseudocolored images of single field of human ileal enteroid expressing GCamP-6s showing areas involved in Ca^{2+} waves over 60 minutes. Different colors were used for each Ca^{2+} wave. If multiple Ca^{2+} waves occurred in the same area, only a single color is shown. (*i*) Irradiated virus. (*ii*) Exosomes. (*iii*) VLPs. (*iv*) VLPs after TMEM16inh-Ao1. Results from a single monolayer are shown using data from Figure 9 and (*C*). To generate the pseudocolored images, all pixels from within the areas of interest, representing the extent of Ca^{2+} waves, were binarized (value 1), then the MetaMorph Stack Topographic Surface Map command was used to generate the figure, which was colorized using MetaMorph Rainbow lookup tables (*blue*, low; *green*, middle; *red*, high). Each of the 1800 time points had a grayscale value (0–255) assigned, then the 8-bit color image was converted to 24-bit color for illustration.

of Spike that is known necessary for Spike fusion and virus entry. Further suggestion that intracellular Ca^{2+} is important for some SARS-CoV-2 cellular effects is based on knockout of STIM1 in HEK294-ACE2-expressing cells that was associated with resistance to SARS-Cov-2 infection, whereas Orai knockout increased this susceptibility.[40]

The VLP-related Ca^{2+} waves were inhibited by apical P2Y1 inhibitor, BPTU. Viral diarrheas have been demonstrated to involve elevation of intracellular Ca^{2+} in enterocytes, with examples including rotavirus, porcine epidemic diarrhea virus, and enterovirus A71,[41–43] whereas multiple other viruses, including poliovirus and coxsackievirus, have been shown to elevate intracellular Ca^{2+} in additional cell types.[42] Best studied has been rotavirus, in which the mechanism of Ca^{2+} elevation and its role in pathogenesis of diarrhea has been characterized in great detail by Hyser and his associates.[42–44] They demonstrated that rotavirus elevated intracellular Ca^{2+} within hours of exposure and this involved spreading of Ca^{2+} waves by a mechanism that involved the viral enterotoxin NSP4, extracellular release of ATP/ADP, based on inhibition by apyrase, and activation of P2Y1 receptors.[43] The unusual aspect of the SARS-CoV-2 VLP initiation of P2YI dependent Ca^{2+} waves in our studies was the rapid activation, within minutes of addition. We assume but have not documented apical secretion of ATP/ADP. Of interest was that the Ca^{2+} response with apyrase and BPTU was lower than untreated or the response to exosomes, suggesting basal apical release of some ATP/ADP. The polarized distribution of the enterocyte P2Y1 receptor has been assumed but not proven to be at the apical surface.

Another unexplored aspect of the VLP initiation of Ca^{2+} elevation is the role of the involved TMEM16 member. We do not present evidence that this is TMEM16F, which has both phosphatidylserine scramblase and Cl^- channel activity[45–49] or explore the potential mechanism of how the involved TMEM16 family member alters intracellular Ca^{2+}. Although TMEM16A has been shown in some studies to cause release of Ca^{2+} from intracellular stores,[49] it did not appear involved in VLP elevation of enteroid Ca^{2+} in the current study.

Limitations for our studies include the need to use surrogates for studying many of the effects of live SARS-CoV-2 in COVID-19 diarrhea in patients. Of note is that the major findings made with live virus were reproduced with the VLPs (partial effects on cytokine release and mRNAs), which also caused pathophysiologic effects on anion secretion and intracellular Ca^{2+}. In addition, the enteroid model only includes epithelial cells. The pathophysiological mechanisms of multiple diarrheal diseases includes the contributions by the inflammatory and immune cells present in the intestinal submucosa/lamina propria. This is highly relevant given the demonstrated ability of SARS-CoV-2 to enter macrophages, which are present in the lamina propria under basal conditions, and release cytokines.[50] Recent studies have allowed enteroid monolayers to be co-cultured with macrophages, dendritic cells, neutrophils, endothelial cells, and components of the ENS, among other cell types.[51,52] These co-culture models have great potential to add insights in the COVID-19 diarrhea pathogenesis in future studies. Concerning the clinical significance of COVID-19 diarrhea, it is usually not severe enough to require large volume replacement and is not life-threatening by itself. Thus, its clinical significance is in predicting a more severe course of acute COVID-19 and a greater risk of developing long COVID. Equally important, however, is the potential relevance of the findings to other inflammatory diarrheas, such as inflammatory bowel diseases, in which effects of longer term elevation of cytokines on transport protein expression and function should be further explored.

Methods

Chemicals, Antibodies, Other Reagents

The general CaCC inhibitor-Ao1 and specific TMEM16A inhibitor-Ao1 and the CFTR inhibitor BPO-27 were gifts provided by A. Verkman.[53–55] Forskolin (cat# 66575-29-9), clotrimazole (cat# 23593-75-1), BAPTA-AM (cat# A1076), apyrase (cat# A6535) (Sigma); IL-6, IL-8 (PepProtech); BPTU (N-[2-[1,1-dimethylethyl)phenoxy]-N'-[trifluoromethoxy)phenyl]urea (TOCRIS, cat# 87054-59-5). Dextran Alexa Fluor 488 (10 kDa), and Alexa Fluor 568 (70 kDa) (Invitrogen). Anti-dsRNA monoclonal antibodies (clone rJ2; Millipore, cat# MABE1134); anti-spike rabbit polyclonal antibodies (ProSci, cat# 3525); anti-NHE3 antibodies (Novus Biologicals, cat# NBP1- 82574); anti-ACE2 – monoclonal mouse IgG2A (R&D Systems, cat# MAB933); anti-GAPDH antibodies (Sigma, cat# G8795); phalloidin and secondary fluorescent AlexaFluor antibodies from Invitrogen. Vero E6 cells (ATCC CRL-1586).

Virus

Live virus: USAWA1/2020 SARS-CoV-2, Spike protein D614G (BEI Resources). Live virus stocks (10^6 PFUs/ml) were inactivated by ultraviolet radiation (103.8 mJ/cm^2) using a Fisherbrand UV crosslinking box. UV inactivation was validated by plaque assay on Vero E6 cells.[22] The radiated virus was concentrated 10× by dialysis using Slide-A-Lyzer @ Cassette Dialysis Cassette (Thermo Scientific, cat# 66383) for 72 hours in phosphate buffered saline (PBS) buffer at 4°C, changing the solution every 24 hours ×3, followed by passage through Amicon Ultra-2ml Centrifugal Filters (Millipore, cat# 0187) to concentration of 1×10^7 PFUs/ml. The virus was aliquoted and stored at −80 °C for single thaw use. The virus was studied at a final concentration of 10^5 to 10^6 PFUs/ml. Live viral studies were performed in a Biosafety Level-3 facility.

VLPs:[29] HEK293F cells were transfected with pS149 and selected in zeocin-containing media, creating the cell line Ftet1, which constitutively expresses the rtTAv16 Tet-on transcription factor from a CMV promoter-driven bicistronic ORF, upstream of a viral peptide and the bleomycin resistance gene. Htet1 cells were converted to SARS-CoV-2 VLP-producing cell lines Ftet1/S226 and Ftet1/CG201 by transfection with Sleeping Beauty transposons that carry 5 separate genes: (1) a puromycin-resistance gene under control of a minimal EF1alpha promoter; (2) SARS-CoV-2 Envelope gene under control of the tetracycline/doxycycline inducible TRE3G promoter; (3) SARS-CoV-2 Membrane gene under control of the TRE3G promoter; (4) SARS-CoV-2 Nucleocapsid gene under control of the TRE3G promoter; and (5) the SARS-CoV-2 Spike/D614G gene under control of the TRE3G promoter (pCG201). Spike-D614G encodes a protein identical to

Spike encoded by the Wuhan-1 strain of SARS-CoV-2 with the exception of the D614G mutation. To generate SARS-CoV-2 VLPs carrying the fusogenic, functional Spike-D614G protein, Ftet1/CG201 cells were grown in suspension cultures in Freestyle media in the presence of 1 ug/ml doxycycline for 3 to 4 days. Starting cell densities were between 0.5 and 1 $\times$ 10^6 cells/ml and the cells were grown in sterile, baffled Erlenmeyer culture flasks at 110 rpm in a humidified, 37 ^oC incubator containing 5% CO_2. VLPs were purified from Ftet1/S226 suspension cell cultures by the following protocol. In brief, cells were removed by centrifugation (5000 $\times$ g for 10 minutes), and the resulting supernatants were sterilized by gravity filtration through a 220-nm pore diameter filtration device, generating clarified tissue culture supernatants. The VLPs were then concentrated $\sim$300-fold by centrifugal filtration of each CTCS across a 100 kDa cutoff membrane ($\sim$160 ml CTCS to a volume of $\sim$0.5 ml). The concentrated VLP-containing suspension was then separated by size exclusion chromatography and VLP-containing fractions were collected, pooled, and quantified by nanoparticle tracking analysis using a ParticleMetrix Zetaview camera according to the manufacturer's instructions. VLP identity was confirmed by immunoblot using antibodies specific for Spike, Membrane, and Envelope.

Enteroid and Colonoid Cultures

A single duodenal, 3 ileal, and 3 ascending colonic enteroid (colonoid) cultures were derived from intestinal biopsies obtained from normal, healthy donors, as previously described.[56–58] Ileal enteroids from a homozygous FΔ508 patient with cystic fibrosis was studied (provided by Hugo deJonge, Erasmus Medical Center). Briefly, human enteroids/colonoids were maintained as 3D spheroids in Matrigel in enteroid expansion media containing the growth factors Wnt3a, R-spondin1, Noggin, and EGF necessary for long-term culture.[39,56–60]

Enteroid/colonoid monolayers were generated by seeding enteroids/colonoids isolated from Matrigel and fragmented by enzymatic digestion onto 24-well Transwell inserts (Corning #3470), as described in detail.[56–58,60] Results were all from studies on human enteroids or colonoids grown as confluent monolayers on Transwell inserts, as we and others have reported previously.[39,56–58,60–63] Sex was not considered as a biological variable.

Enteroid/Colonoid Infection

Confluent enteroid/colonoid monolayers were studied in the undifferentiated state in the presence of conditioned media with Wnt3a, R-spondin1, and Noggin and in the differentiated state, 5 to 6 days after removal of Wnt, R-spondin1, and Noggin, as reported.[56] Enteroids were inoculated apically with either 10^5 or 10^6 PFUs/ml live SARS-CoV-2 virus (isolate USAWA1/ 2020 SARS-CoV-2; BEI Resources) for 90 minutes; apical media was then replaced by virus-free media, and the infection was monitored for up to 5 days. For studies with VLPs, apical exposure was with 10^6 to 10^8 particles/ml.

Plaque Assay for Live Virus

SARS-CoV-2 plaque assays in Vero E6 cells were used to assess viral replication. Vero E6 cells were incubated in a 24-well plate until they reached 90% confluency. Supernatants from enteroid cultures were mixed with media and added to cells for 2 hours. The supernatants were removed, and the cells were overlaid with media comprised of equal volumes of (1) minimal essential medium/5% FCS/2$\times$ antibiotics and (2) 2% agarose. After 2 days, the overlay was removed, cells were stained with crystal violet, and plaques were counted.

qRT-PCR

Human enteroid monolayers cultured in Transwell inserts were exposed to either live virus, irradiated virus, or VLPs (empty exosome were used as negative control) apically, and, when used, IL-6 plus IL-8 (50 ng/ml each) were added to the basolateral surface. For the live virus studies, the virus was washed out after 90 minutes, and studies were performed at 48 or 120 hours. Detection of SARS-CoV-2 was by qRT-PCR. Presence of SARS-CoV-2 in enteroids and colonoids, as well as in apical and basolateral media, was determined using primers and probes (N1, N2, and RP) from the CDC 2019 real-time RT-PCR diagnostic panel (IDT). Positive controls used in these reactions included SARS-CoV-2 RNA (WA1-USA strain, from UTMB) as well as the 2019-nCoV-N and the Hs-RPP30 control plasmids (IDT). RT-qPCR were performed using TaqPath 1-stepq RT-PCR master mix (ThermoFisher) on the ABI StepOnePlus Real-Time PCR system. Reverse transcription and amplification conditions were 25 ^oC for 2 minutes, 50 ^oC for 15 minutes, and 95 ^oC for 2 minutes, followed by 45 cycles of 95 ^oC for 3 seconds and 55 ^oC for 30 seconds.

Irradiated virus (10^5–10^6 PFU/ml) or VLPs (10^6–10^8 particles/ml) were added apically at time 0 and 24 hours. Forty-eight hours after the initial viral addition, the apical and basolateral media were collected, the apical surface of the enteroids was washed twice with PBS, the enteroids were scraped off the inserts, resuspended in PBS, and centrifuged at 5000 rpm $\times$ 5 min. Total RNA from the scraped enteroids and apical and basolateral media were isolated using PureLink RNA Mini kit (Invitrogen, cat# 12183018A) according to the manufacturer's protocol. cDNA was synthesized using SuperScript VILO Master Mix (Invitrogen, cat# 11756050). qRT-PCR was performed using PowerUp SYBR Green Master Mix (Applied Biosystems, cat# A25742) on a QuantStudio 12 K Flex real-time PCR system (Applied Biosystems). The sequences of gene-specific primers are listed in Table 1. Each sample was studied in duplicate. Human GAPDH gene was used as the internal control for normalization. Results were quantitated using the 2–ΔΔCT method. The basolateral media were also used for cytokine assays.

Cytokine Assays

The media from live virus/VLP/irradiated virus exposed media were used for cytokine assays. Cytokine/chemokine levels were assayed using the U-Plex Human Biomarker

Table 1. Gene-specific Primers for qRT-PCR

Gene	Forward (5′-3′)	Reverse (5′-3′)
DRA	CCATCATCGTGCTGATTGTC	AGCTGCCAGGACGGACTT
CFTR	GAAGTAGTGATGGAGAATGTAACAGC	GCTTTCTCAAATAATTCCCCAAA
NHE3	GTCTTCCTCAGTGGGCTCAT	ATGAGGCTGCCAAACAGG
TMEM16A	ATCAGCCAGCAGATCCACAAG	GCTCCTTCTCCATCCAGGTTT
TMEM16F	TCCGTCCCTCCCTACGGGGA	AGCCAGCTTGGCTGCAATCACA
GAPDH	ACCCACTCCTCCACCTTTGA	CTGTTGCTGTAGCCAAATTCGT

qRT-PCR, Quantitative reverse transcription polymerase chain reaction.

Group 1 (cat# K15067L-1, MesoScale Diagnostics). Wells were washed 3 times with MSD Wash Buffer before incubation with detection antibody solution for 1 hour at room temperature, with shaking. Wells were washed again 3 times before adding 150 μl of Read Buffer T to each well. Measurements were obtained on MESO Quickplex SQ 120 Imager using Discover Workbench 4.0 software (MesoScale Diagnostics).

Immunoblotting

Enteroids were collected from the Transwell inserts as described in the qRT-PCR description and solubilized in lysis buffer containing 60 mM hydroxyethyl piperazine ethanesulfonic acid (HEPES), 150 mM NaCl, 3 mM KCl, 5 mM EDTA trisodium, 3 mM EGTA, 1 mM Na_3PO_4, a protease inhibitor cocktail (Sigma-Aldrich, cat# P8340) in 1% Triton X-100. Protein lysates were passed through a 1-ml syringe 23-gauge needle 15 times and centrifuged at 10,000 g for 15 minutes, and protein was quantitated using the bicinchoninic acid method. Proteins were then separated on 10% SDS-PAGE gels and transferred onto a nitrocellulose membrane. The blot was blocked with 5% nonfat milk for 1 hour, then probed with primary antibodies, in blocking buffer overnight at 4 °C, followed by secondary antibody against mouse or rabbit for 1 hour at room temperature. Protein bands were visualized and quantitated using an Odyssey system and Image Studio software (LI-COR Biosciences).

Immunofluorescence

Enteroids on Transwell inserts were rinsed with PBS and fixed in 4% paraformaldehyde for 30 minutes at 4 °C. After being blocked/permeabilized by 5% bovine serum albumin and 0.1% saponin, cells were incubated with primary antibodies overnight at 4 °C. The next day, cells were incubated with Hoechst 33342 (Thermo Fisher) and secondary antibodies conjugated with Alexa Fluor 488 or 568 for 1 hour at room temperature. Finally, cells were visualized using an Olympus FV3000RS confocal microscope with a silicon oil objective (×30, NA 1.05).

Active Anion Secretion[64]

Ussing Chamber/Voltage Clamp Studies. Ileal monolayers were grown on Transwell inserts and were maintained in the undifferentiated state. These ileal monolayers were switched overnight to CMGF negative medium (Advanced DMEM/F12 medium containing GlutaMAX [2 mmol/L] and HEPES [10 mmol/L]) either with or without 50 ng/ml each of IL-6 and IL-8. On the day of experiments, these Transwell inserts were mounted in Ussing chambers (Physiological Instruments). The apical and basolateral hemichambers were filled with buffer that was gassed continuously with 95% O_2/5% CO_2, maintained at 37 °C, and connected to a voltage clamp apparatus (Physiological Instruments) via Ag/AgCl electrodes and 3 Mol/L KCl agar bridges. Krebs-Ringer bicarbonate buffer consisted of 115 mmol/L NaCl, 25 mmol/L NaHCO3, 0.4 mmol/L KH2PO4, 2.4 mmol/L K2HPO4, 1.2 mmol/L CaCl2, and 1.2 mmol/L MgCl2, pH 7.4. In addition, buffer in the basolateral hemichamber was supplemented with 4 mmol/L glucose as an energy substrate; buffer in the apical hemichamber was supplemented with 4 mmol/L mannitol to maintain the osmotic balance. To investigate the effect of VLP S-D614G on anion secretion, VLPs were added to the apical chamber with several protocols. In most studies, the VLP particles were added one time with a concentration of 3×10^8 /ml to the apical chamber; in other studies, 10^8 particles/ml were added sequentially 3 times. Roles of CaCC, CFTR, and K channels in the VLP D614G stimulated increase in short-circuit current (Isc) (representing stimulated electrogenic anion secretion) were studied with a general CaCC inhibitor ($CaCC_{inh}$-A01, 20 umol/l) and a TMEM16A specific inhibitor ($TMEM16A_{inh}$-AO1, 25 umol/l), a CFTR inhibitor (BPO-27, 1 μmol/l), and a K channel blocker (clotrimazole, 30 um/l). The effect of BAPTAM-AM (35 umol/l) was with 30 minutes preincubation. The peak increase in Isc that occurred above baseline was considered the maximum anion secretion achieved. In some cases, IL-6 plus IL-8 (each 50 ng/ml) were added to the enteroid basolateral media ∼18 to 20 hours before active ion transport was determined.

Stable Expression of GCamP-6s

Plasmid pGP-CMV-GCaMP-6s (Addgene plasmid 40753; http://addgene.org/40753) with at least 10^6 viral particles was cloned into lentiviral vector pCDH-EF1-MCS-IRES (puro) and lentiviral particles produced and transduced into normal human ileal enteroids that were then selected with puromycin (0.5 mg/ml). Clones with the highest expression were selected for study. The selected enteroids were grown as a confluent undifferentiated monolayer on polyethelene Transwell filters in 12-well plates

Ca^{2+} Imaging and Quantitation

Ileal enteroid monolayers expressing GCamP-6s confirmed as having nearly uniform expression were selected for study. Live images of GCaMP-6s fluorescence were obtained with an Olympus FV3000RS confocal microscope (10× objective lens, NA 0.40; 2.00 digital zoom); resonant scan with 16 frame average; 0.3 um step size; pinhole 2.3 Airy units at 37 °C using an OkoLab stage top plus transparent shroud incubator at 37 °C under 5% CO_2 atmosphere. Time lapse images were taken once every 2 seconds for 60 minutes.

Olympus FV3000RS confocal microscopy time series (.OIR files, 512 × 512 pixels, 637 × 637 um, 1.243 um/pixel, 2-second interval) were exported using the Olympus FV31-SW, v2.1.1.98 acquisition software to TIFF series (1800 time points for 1 hour data), opened in MetaMorph Imaging System 7.7.3.0 as an image stack, median 5 × 5 filtered and saved. A 500 × 500-pixel region of interest (.rgn file) was used. The image stack was examined, each Ca^{2+} ion "wave" event was identified, and a region of interest was drawn around the entire event (excluding image edge pixels that had not been median filtered). Waves needed to be at least 3 to 5 cells in size to be considered a wave, and quantitation only considered elevation in Ca^{2+} in a wave of >500 pixels. Identical events and smaller events entirely within larger events were counted as 1 wave. Overlapping wave events were each assigned regions, which led to some highly active image stacks having greater total wave region areas than the size of the original image. For the cells in waves, the initial cell elevating Ca^{2+} was identified, and the time course of Ca^{2+} elevation examined starting from time of VLP addition. Data were exported from MetaMorph's software Measure Regions (area of each region) and Graph Intensities (average intensity of each region for every time point) determined using Windows 10 dynamic data exchange to Microsoft Excel 2016 and saved in XLSX file format before being transferred to Prism 8/9 for graphing and analysis.

Statistical Analyses

Experiments were generally repeated 3 to 5 times and tested for statistical significance with the Student's paired or unpaired *t*-tests or via analysis of variance (ANOVA) with Bonferroni's post-test (GraphPad) when 3 or more comparisons were carried out. P values of $< .05$ were considered statistically significant.

Study Approval

Generation and study of human enteroids were approved by the institutional review boards of Johns Hopkins University School of Medicine (NA_00038329) and University of New Mexico School of Medicine (18-171).

Supplementary Material

Note: To access the supplementary material accompanying this article, visit the online version of Cellular and Molecular Gastroenterology and Hepatology at www.cmghjournal.org, and at https://doi.org/10.1016/j.jcmgh.2024.101383.

References

1. Friedel DM, Cappell MS. Diarrhea and coronavirus disease 2019 infection. Gastroenterol Clin North Am 2023; 52:59–75.
2. Freedberg DE, Chang L. Gastrointestinal symptoms in COVID-19: the long and the short of it. Curr Opin Gastroenterol 2022;38:555–561.
3. Zarifian A, Zamiri Bidary M, Arekhi S, et al. Gastrointestinal and hepatic abnormalities in patients with confirmed COVID-19: a systematic review and meta-analysis. J Med Virol 2021;9:336–350.
4. D'Amico F, Baumgart DC, Danese S, Peyrin-Biroulet L. Diarrhea during COVID-19 infection: pathogenesis, epidemiology, prevention, and management. Clin Gastroenterol Hepatol 2020;18:1663–1672.
5. Redd WD, Zhou JC, Hathorn KE, et al. Prevalence and characteristics of gastrointestinal symptoms in patients with severe acute respiratory syndrome coronavirus 2 infection in the United States: a multicenter cohort study. Gastroenterology 2020;159:765–767.e2.
6. Wong SH, Lui RN, Sung JJ. Covid-19 and the digestive system. J Gastroenterol Hepatol 2020;35:744–748.
7. Wei XS, Wang X, Niu YR, et al. Diarrhea is associated with prolonged symptoms and viral carriage in Corona Virus disease 2019. Clin Gastroenterol Hepatol 2020; 18:1753–1759.e2.
8. Tian Y, Rong L, Nian W, He Y. Review article: gastrointestinal features in COVID-19 and the possibility of faecal transmission. Aliment Pharmacol Ther 2020;51:843–851.
9. Han C, Duan C, Zhang S, et al. Digestive symptoms in COVID-19 patients with mild disease severity: clinical presentation, stool viral RNA testing, and outcomes. Am J Gastroenterol 2020;115:916–923.
10. Comoglu Ş, Öztürk S, Kant A, et al. Evaluation of diarrhea in patients with Covid-19. Dig Dis 2021;39:622–625.
11. Alonso-Navarro R, Ramírez M, Masiá M, et al. Time from symptoms onset to remdesivir is associated with the risk of ICU admission: a multicentric analyses. BMC Infect Dis 2023;23:286.
12. Lopez-Leon S, Wegman-Ostrosky T, Perelman C, et al. More than 50 long-term effects of COVID-19: a systematic review and meta-analysis. medRxiv 2021. https://doi.org/10.1101/2021.01.27.21250617.
13. Cheung CCL, Goh D, Lim X, et al. Residual SARS-CoV-2 viral antigens detected in GI and hepatic tissues from five recovered patients with COVID-19. Gut 2022;71:226–229.
14. Augustin M, Schommers P, Stecher M, et al. Post-COVID syndrome in non-hospitalised patients with COVID-19: a longitudinal prospective cohort study. Lancet Reg Health Eur 2021;6:100122.
15. Aiyegbusi OL, Hughes SE, Turner G, et al; TLC Study Group. Symptoms, complications and management of long COVID: a review. J R Soc Med 2021;114:428–442.
16. Deinhardt-Emmer S, Wittschieber D, Sanft J, et al. Early postmortem mapping of SARS-CoV-2 RNA in patients with COVID-19 and the correlation with tissue damage. Elife 2021;10:e60361.
17. Skok K, Stelzl E, Trauner M, Kessler HH, Lax SF. Postmortem viral dynamics and tropism in COVID-19 patients

in correlation with organ damage. Virchows Arch 2021; 478:343–353.
18. Zang R, Gomez Castro MF, McCune BT, et al. TMPRSS2 and TMPRSS4 promote SARSCoV 2 infection of human small intestinal enterocytes. Sci Immunol 2020;5:eabc3582.
19. Rao MC. Physiology of electrolyte transport in the gut: implications for disease. Compr Physiol 2019;9:947–1023.
20. Camilleri M, Sellin JH, Barrett KE. Pathophysiology, evaluation, and management of chronic watery diarrhea. Gastroenterology 2017;152:515–532.e2.
21. Binder HJ. Pathophysiology of acute diarrhea. Am J Med 1990;88:2S–4S.
22. Heilingloh CS, Aufderhorst UW, Schipper L, et al. Susceptibility of SARS-CoV-2 to UV irradiation. Am J Infect Control 2020;48:1273–1275.
23. Wang Y, Perlman S. COVID-19: inflammatory profile. Annu Rev Med 2022;73:65–80, 27.
24. Ragab D, Salah Eldin H, Taeimah M, Khattab R, Salem R. The COVID-19 cytokine storm; what we know so far. Front Immunol 2020;11:1446.
25. Giannakodimos I, Gkountana GV, Lykouras D, Karkoulias K, Tsakas S. The role of interleukin-6 in the pathogenesis, prognosis and treatment of severe COVID-19. Curr Med Chem 2021;28:5328–5338.
26. Coperchini F, Chiovato L, Rotondi M. Interleukin-6, CXCL10 and infiltrating macrophages in COVID-19-related cytokine storm: not one for all but all for one! Front Immunol 2021;12:668507.
27. Andargie T, Zhou W, Karaba A, et al. Integrated cell-free DNA and cytokine analysis uncovers distinct tissue injury and immune response patterns in solid organ transplant recipients with COVID-19. Res Sq 2022:rs.3.rs-1262270.
28. Karaba AH, Zhou W, Hsieh LL, et al. Differential cytokine signatures of severe acute respiratory syndrome coronavirus 2 (SARS-CoV-2) and influenza infection highlight key differences in pathobiology. Clin Infect Dis 2022;74:254–262.
29. Donowitz M, Tse CM, Dokladny K, et al. SARS-COV-2 induced diarrhea is inflammatory, Ca 2+ dependent and involves activation of calcium activated Cl channels. bioRxiv 2021. https://doi.org/10.1101/2021.04.27.441695.
30. Salari A, Xiu R, Amiri M, et al. The anion channel TMEM16a/Ano1 modulates CFTR activity, but does not function as an apical anion channel in colonic epithelium from cystic fibrosis patients and healthy individuals. Int J Mol Sci 2023;24:14214.
31. Benedetto R, Cabrita I, Schreiber R, Kunzelmann K. TMEM16A is indispensable for basal mucus secretion in airways and intestine. FASEB J 2019;33:4502–4512.
32. Ousingsawat J, Kongsuphol P, Schreiber R, Kunzelmann K. CFTR and TMEM16A are separate but functionally related Cl- channels. Cell Physiol Biochem 2011;28:715–724.
33. Kunzelmann K, Centeio R, Wanitchakool P, et al. Control of ion transport by Tmem16a expressed in murine intestine. Front Physiol 2019;10:1262.
34. Salari A, Xiu R, Amiri M, et al. The anion channel TMEM16a/Ano1 modulates CFTR activity, but does not function as an apical anion channel in colonic epithelium from cystic fibrosis patients and healthy individuals. Int J Mol Sci 2023;24:14214.
35. Benedetto R, Ousingsawat J, Wanitchakool P, et al. epithelial chloride transport by CFTR requires TMEM16A. Sci Rep 2017;7:12397.
36. Ousingsawat J, Martins JR, Schreiber R, Rock JR, Harfe BD, Kunzelmann K. Loss of TMEM16A causes a defect in epithelial Ca2+-dependent chloride transport. J Biol Chem 2009;284:28698–28703.
37. Lee B, Hong GS, Lee SH, et al. Anoctamin 1/TMEM16A controls intestinal Cl- secretion induced by carbachol and cholera toxin. Exp Mol Med 2019;51:1–14.
38. Sim JR, Shin DH, Park PG, et al. Amelioration of SARS-CoV-2 infection by ANO6 phospholipid scramblase inhibition. Cell Rep 2022;40:111117.
39. In J, Foulke-Abel J, Zachos NC, et al. Enterohemorrhagic Escherichia coli reduce mucus and intermicrovillar bridges in human stem cell-derived colonoids. Cell Mol Gastroenterol Hepatol 2016;2:48–62.e3.
40. Wu B, Ramaiah A, Garcia G Jr, Hasiakos S, Arumugaswami V, Srikanth S. ORAI1 limits SARS-CoV-2 infection by regulating tonic type I IFN signaling. J Immunol 2022;208:74–84.
41. Guo X, Feng Y, Zhao X, et al. Coronavirus porcine epidemic diarrhea virus utilizes chemokine interleukin-8 to facilitate viral replication by regulating Ca2+ flux. J Virol 2023;97:e0029223.
42. Hyser JM, Estes MK. Pathophysiological consequences of calcium-conducting viroporins. Annu Rev Virol 2015; 2:473–496.
43. Chang-Graham AL, Perry JL, Engevik MA, et al. Rotavirus induces intercellular calcium waves through ADP signaling. Science 2020;370:eabc3621.
44. Chang-Graham AL, Perry JL, Strtak AC, et al. Rotavirus calcium dysregulation manifests as dynamic calcium signaling in the cytoplasm and endoplasmic reticulum. Sci Rep 2019;9:10822.
45. Pelz T, Drose DR, Fleck D, et al. An ancestral TMEM16 homolog from Dictyostelium discoideum forms a scramblase. PLoS One 2018;13:e0191219.
46. Feng S, Dang S, Han TW, et al. Cryo-EM studies of TMEM16F calcium-activated ion channel suggest features important for lipid scrambling. Cell Rep 2019;28:567–579.e4.
47. Kunzelmann K, Nilius B, Owsianik G, et al. Molecular functions of anoctamin 6 (TMEM16F): a chloride channel, cation channel, or phospholipid scramblase? Pflugers Arch 2014;466:407–414.
48. Deisl C, Hilgemann DW, Syeda R, Fine M. TMEM16F and dynamins control expansive plasma membrane reservoirs. Nat Commun 2021;12:4990.
49. Cabrita I, Benedetto R, Fonseca A, et al. Differential effects of anoctamins on intracellular calcium signals. FASEB J 2017;31:2123–2134.
50. Pantazi I, Al-Qahtani AA, Alhamlan FS, et al. SARS-CoV-2/ACE2 interaction suppresses IRAK-M expression and promotes pro-inflammatory cytokine production in macrophages. Front Immunol 2021;12:683800.
51. Noel G, Baetz NW, Staab JF, et al. A primary human macrophage-enteroid co-culture model to investigate mucosal gut physiology and host-pathogen interactions. Sci Rep 2017;7:45270.

52. Lemme-Dumit JM, Doucet M, Zachos NC, Pasetti MF. Epithelial and neutrophil interactions and coordinated response to *Shigella* in a human intestinal enteroid-neutrophil coculture model. mBio 2022;13:e0094422.
53. Kumar S, Namkung W, Verkman AS, Sharma PK. Novel 5-substituted benzyloxy-2-arylbenzofuran-3-carboxylic acids as calcium activated chloride channel inhibitors. Bioorg Med Chem 2012;20:4237–4244.
54. Piechowicz KA, Truong EC, Javed KM, et al. Synthesis and evaluation of 5,6-disubstituted thiopyrimidine aryl aminothiazoles as inhibitors of the calcium-activated chloride channel TMEM16A/Ano1. J Enzyme Inhib Med Chem 2016;31:1362–1368.
55. Truong EC, Phuan PW, Reggi AL, et al. Substituted 2-acylaminocycloalkylthiophene-3-carboxylic acid arylamides as inhibitors of the calcium-activated chloride channel transmembrane protein 16A (TMEM16A). J Med Chem 2017;60:4626–4635.
56. Yin J, Tse CM, Avula LR, et al. Molecular basis and differentiation-associated alterations of anion secretion in human duodenal enteroid monolayers. Cell Mol Gastroenterol Hepatol 2018;5:591–609.
57. Foulke-Abel J, In J, Yin J, et al. Human enteroids as a model of upper small intestinal ion transport physiology and pathophysiology. Gastroenterology 2016;150:638–649.e8.
58. In JG, Foulke-Abel J, Estes MK, Zachos NC, Kovbasnjuk O, Donowitz M. Human mini-guts: new insights into intestinal physiology and host-pathogen interactions. Nat Rev Gastroenterol Hepatol 2016;13:633–642.
59. Zachos NC, Kovbasnjuk O, Foulke-Abel J, et al. Human enteroids/colonoids and intestinal organoids functionally recapitulate normal intestinal physiology and pathophysiology. J Biol Chem 2016;291:3759–3766.
60. Yin J, Sunuwar L, Kasendra M, et al. Fluid shear stress enhances differentiation of jejunal human enteroids in intestine-chip. Am J Physiol Gastrointest Liver Physiol 2021;320:G258–G271.
61. Johnson K, Yin J, In JG, et al. Cholinergic-induced anion secretion in murine jejunal enteroids involves synergy between muscarinic and nicotinic pathways. Am J Physiol Cell Physiol 2020;319:C321–C330.
62. Singh V, Johnson K, Yin J, et al. Chronic inflammation in ulcerative colitis causes long-term changes in goblet cell function. Cell Mol Gastroenterol Hepatol 2022;13:219–232.
63. Liu L, Saitz-Rojas W, Smith R, et al. Mucus layer modeling of human colonoids during infection with enteroaggragative E. coli. Sci Rep 2020;10:10533.
64. Tse CM, In JG, Yin J, et al. Enterohemorrhagic E. coli (EHEC)-secreted serine protease EspP stimulates electrogenic ion transport in human colonoid monolayers. Toxins (Basel) 2018;10:351.

Received January 29, 2024. Accepted July 23, 2024.

Correspondence
Address correspondence to: Mark Donowitz, MD; The Johns Hopkins University School of Medicine; Ross 925; 720 Rutland Ave; Baltimore, Maryland 21205. e-mail: mdonowit@jhmi.edu.

CRediT Authorship Contributions

Mark Donowitz, MD (Conceptualization: Lead; Formal analysis: Supporting; Funding acquisition: Lead; Methodology: Lead; Project administration: Lead; Resources: Lead; Supervision: Supporting; Validation: Supporting; Writing – original draft: Lead; Writing – review & editing: Lead)

Chung Ming Tse, PhD (Data curation: Supporting; Formal analysis: Equal; Funding acquisition: Equal; Investigation: Equal; Methodology: Lead; Resources: Supporting; Supervision: Supporting; Validation: Supporting; Writing – original draft: Supporting; Writing – review & editing: Supporting)

Rafiquel Sarker, PhD (Formal analysis: Supporting; Investigation: Supporting; Validation: Supporting; Writing – review & editing: Supporting)

Ruxian Lin, MS (Data curation: Supporting; Formal analysis: Supporting; Investigation: Supporting; Writing – review & editing: Supporting)

Karol Dokladmy, MS (Data curation: Supporting; Investigation: Supporting; Writing – review & editing: Supporting)

Manmeet Rawat, PhD (Data curation: Supporting; Investigation: Supporting; Writing – review & editing: Supporting)

Ivy Horwitz, PhD (Data curation: Supporting; Formal analysis: Supporting; Investigation: Supporting; Writing – review & editing: Supporting)

Chun Yan Ye, PhD (Data curation: Supporting; Formal analysis: Supporting; Investigation: Supporting; Writing – review & editing: Supporting)

George McNamara, PhD (Formal analysis: Equal; Methodology: Supporting; Writing – review & editing: Supporting)

Julie In, PhD (Data curation: Supporting; Investigation: Supporting; Validation: Supporting; Writing – review & editing: Supporting)

Alison Kell, PhD (Data curation: Supporting; Formal analysis: Supporting; Investigation: Supporting; Writing – review & editing: Equal)

Chenxu Guo, PhD (Formal analysis: Supporting; Investigation: Supporting; Writing – review & editing: Supporting)

Shang Jui Tsai, PhD (Investigation: Supporting; Methodology: Supporting; Validation: Supporting; Writing – review & editing: Supporting)

Tyrus Vong, MS (Data curation: Supporting; Formal analysis: Supporting; Investigation: Supporting; Writing – review & editing: Supporting)

Andrew Karaba, MD, PhD (Data curation: Equal; Formal analysis: Supporting; Investigation: Supporting; Writing – review & editing: Supporting)

Varsha Singh, PhD (Data curation: Supporting; Formal analysis: Supporting; Investigation: Equal; Writing – review & editing: Supporting)

Jaiprasath Sachithanandham, PhD (Data curation: Supporting; Investigation: Supporting; Methodology: Supporting)

Andy Pekosz, PhD (Formal analysis: Supporting; Methodology: Supporting; Supervision: Supporting; Writing – review & editing: Supporting)

Andrea Cox, MD, PhD (Data curation: Supporting; Formal analysis: Supporting; Methodology: Supporting; Supervision: Supporting; Writing – review & editing: Supporting)

Steven Bradfute, PhD (Formal analysis: Supporting; Funding acquisition: Supporting; Investigation: Supporting; Methodology: Supporting; Resources: Supporting; Supervision: Supporting; Writing – review & editing: Supporting)

Nicolas C. Zachos, PhD (Conceptualization: Supporting; Data curation: Supporting; Formal analysis: Supporting; Investigation: Supporting; Methodology: Supporting; Project administration: Supporting; Resources: Supporting; Supervision: Supporting; Validation: Supporting; Writing – original draft: Supporting; Writing – review & editing: Supporting)

Stephen Gould, PhD (Conceptualization: Supporting; Formal analysis: Supporting; Funding acquisition: Supporting; Investigation: Supporting; Methodology: Supporting; Resources: Supporting; Supervision: Supporting; Writing – original draft: Supporting; Writing – review & editing: Supporting)

Olga Kovbasnjuk, PhD (Conceptualization: Equal; Data curation: Equal; Formal analysis: Supporting; Funding acquisition: Supporting; Investigation: Supporting; Methodology: Supporting; Project administration: Supporting; Resources: Supporting; Software: Supporting; Supervision: Supporting; Validation: Supporting; Writing – original draft: Supporting; Writing – review & editing: Supporting)

Conflicts of interest
The authors disclose no conflicts.

Funding
This study was supported in part by Johns Hopkins University School of Medicine Dean's Durso support, National Institutes of Health/National Institute of Diabetes and Digestive and Kidney Diseases RO1 DK26523, RO1 DK116352, and Digestive Disease Research Core Center Grant P30 DK089502.

Data availability
All data will be made available upon request via request to the corresponding author.